Mon. Not. R. Astron. Soc. **000**, 000–000 (0000) Printed February 25, 2013 (MN LaTeX style file v2.2)

arXiv:1302.5462v1 [astro-ph.CO] 22 Feb 2013

Dark Matter annihilation energy output and its effects on the high-z IGM

Ignacio J. Araya[1] and Nelson D. Padilla[2]
[1] *Department of Physics and Astronomy, University of Southern California, 920 Bloom Walk, Los Angeles, California, U.S.*
[2] *Departamento de Astronomía y Astrofísica, Pontificia Universidad Católica de Chile, Av. Vicuña Mackenna 4860, Stgo., Chile*

February 25, 2013

ABSTRACT

We study the case of DM self annihilation, in order to asses its importance as an energy injection mechanism, to the IGM in general, and to the medium within particular DM haloes. We explain the fact that for thermal relic WIMPS, the annihilation cross section is model independent (except for possible low velocity enhancements), and we consider two well motivated WIMP candidates, the SUSY neutralino and the first KK excited state of the B electroweak boson (also called the KK-photon), that have masses in the range favoured by both, indirect searches and accelerator constraints ($m_\chi \gtrsim 100GeV$). We give an overview of the physical scenarios in which these particles arise, mentioning the motivations and general aspects of the underlying physical theories. We then analyse in detail the clustering properties of CDM, on all hierarchy levels, from haloes to subhaloes and DM density profiles within them. In this analysis, we use the Press-Schechter formalism to compute the DM halo mass function, we consider the subhalo mass function calibrated from N-body simulations, and we also consider the process of adiabatical compression by the presence of a SMBH for our computations. We then explicitly compute the energy output (or luminosity) of DM haloes due to annihilations, and compare the obtained luminosities with the standard AGN feedback process, concluding that DM annihilation does not provide the necessary output as to constitute an important feedback mechanism. We then compute the energy injection rate per baryon of annihilations on the IGM, in order to calculate the effects that it has on its temperature and ionization fraction. We find significant deviations in the evolutions of the temperature and ionization fraction of the IGM, in scenarios that take into account the clustering of DM at all levels, such that a $1TeV$ WIMP may, for example, maintain the temperature of the IGM on the $\sim 100K$ level, or contribute to the ionization fraction maintaining it in a value of $\sim 10^{-2}$ (not considering POPIII stars). We conclude that although the DM annihilation can have a significant impact on the properties of the IGM, it cannot be regarded as an alternative reionization scenario. Regarding the detectability of the WIMP through the modifications to the 21 cm differential brightness temperature signal (δT_b), we conclude that, considering the adiabatic compression and the substructure, and assuming a maximal absorption fraction of $f_{abs} = 1$, a $1TeV$ WIMP with thermal relic cross section may be detected with a peak signal of $\sim 18mK$ at a redshift of ~ 50, corresponding to a frequency of 30MHz.

Key words: Cosmology - Dark Matter - Dark Ages - High-z IGM

1 INTRODUCTION

The Dark Matter (DM) is a component of the total density of the universe which can be measured only through gravitational interactions and (likely) weak interactions. It behaves as dust-like matter in the sense that it is collisionless and that its energy density decreases as the third power of the scale factor. There are many compelling evidences of its existence, although all of them are indirect. These are mainly dynamical evidences, which rely on the gravitational influence of DM. Some examples of these evidences are the rotation curves of late type galaxies (Rubin & Ford 1970), galaxy cluster dynamics (Zwicky 1933) and strong lensing (Paczyński 1987), among others. The effects of DM are very important not only for determining the dynamics of galaxies or galaxy clusters, but also for the evolution of the universe as a whole, and for the galaxy formation processes and structure formation scenarios.

For example, assuming that the DM consists of particles that were originally in thermal equilibrium with the radiation in the early universe, depending on the mass of the particles, the structure formation scenario will be top down or hierarchical. In the top down structure formation scenario, the first structures to collapse are large (on the mass scale that corresponds to present-day superclusters), because all overdensities at smaller scales are erased by free streaming. This is the case for a hot dark matter (HDM) model, in which the DM particles were relativistic at the time of decoupling. In the hierarchical structure formation scenario, small (and also large) structures start to collapse after decoupling, because DM particles were non-relativistic at the time of decoupling, and so the free streaming is negligible. This is the case for a cold dark matter (CDM) model (Blumenthal 1984).

The postulated CDM particle has been named a WIMP (or Weakly Interacting Massive Particle), because it weakly couples to normal matter (for introductions to the topic of DM astrophysics, see D'Amico, Kamionkowski & Sigurdson (2009) and Raffelt (2008)). In the standard scenario, this particle is considered to be a thermal relic. This means that its creation and annihilation processes from the early universe radiation field were in thermal equilibrium with each other, and thus, the present day DM number density is the relic abundance after the freeze-out of this processes, with annihilation being favoured after the universe had cooled enough (Kolb & Turner 1990). This fact alone allows for the computation of the interaction cross section for the creation-annihilation process given only the present day abundance of DM (its density parameter $\Omega_{m,0}$).

There are several DM candidates and scenarios that allow for the existence of a thermal relic WIMP. One of the most highly motivated is the Supersymetric Lightest Neutralino (or simply neutralino), corresponding to the lightest mass eigenstate of the neutral supersymmetric partners of the Standard Model electroweak gauge bosons and Higgses (see for example Martin (2008); and Jungman, Kamionkowski & Griest (1996)). In Supersymmetric theories (called SUSY in general), there is one boson for every fermion and the corresponding partners are called superpartners. As the gauge bosons are vector bosons and the higgses are scalar bosons, the corresponding superpartners are fermions. In SUSY, the neutralino is a Majorana fermion, meaning that it is its own anti-particle, and thus it can annihilate with itself. Also, in R-parity conserving models, the neutralino is stable because no supersymmetric particle is allowed to decay into standard model particles. Thus, the SUSY neutralino may provide a suitable thermal relic WIMP candidate.

Another highly motivated DM candidate is the Lightest Kaluza Klein (LKK) excited state. This corresponds to excitations of standard model particles but in a higher dimensional space coordinate. Spatial extra dimensions is a prediction of several beyond-standard-model physical theories, for example Superstring Theory. In this theories, the extra space dimensions are compactified, so that the effective theory in the low energy limit is four dimensional. Because of the compactified nature of these dimensions, the momentum in them is discreet, and in the effective theory this extra momentum will take the form of an additional contribution to the rest-mass of the particle. KK particles are thus heavy, and conservation of momentum in the extra dimension guarantees that they are stable. For giving an appropriate WIMP, charge neutrality is also required, and thus, the best KK candidate for the WIMP is the $B^{(1)}$ (the first excited state of the B gauge boson, roughly equivalent to the first excited state of the photon). The KK WIMP is a boson, whereas the SUSY WIMP is a fermion, however both are their own anti-particle and thus can annihilate with themselves (Hooper & Profumo 2007).

An important feature of a self-annihilating thermal relic WIMP is that the annihilation products are standard model particles, and thus, they may inject energy to the IGM or to the medium where a particular DM halo is embedded. Globally, the annihilations of WIMPS are unlikely to occur because their abundance has long ago frozen. However, there may be regions where encounters among WIMPS are more probable due to an enhanced density. These regions are precisely the regions where structures form. It is a direct consequence of the ΛCDM model that DM is clumpy, due to the hierarchical growth of structure. Thus, it is precisely in the inner regions of DM haloes and substructures that the annihilations are more probable. The energy output due to annihilations will be proportional to the square of the density, thus, these local density enhancements are of great importance (Natarajan, Croton & Bertone 2008).

The first hierarchy in density enhancements are the DM haloes that do not belong to any gravitationally bound structure at a particular redshift. In N-body DM only simulations, these are called main haloes. An analytic formalism to quantify the number density of these haloes per decade in mass is given by the Press-Schechter formalism (Press & Schechter (1974); Mo & White (1996); Bond et al. (1991); Sheth, Mo & Tormen (2001); Lacey & Cole (1993) among others). This formalism considers that the overdensity field of the universe is a gaussian field, and thus, the properties of its fourier transform are known. One can define the matter power-spectrum as the square of the complex modulus of the overdensity in k space, and compute the variance of the matter fluctuations of scales of a given mass, as a window-smoothed average of the power spectrum on the corresponding volume. The Press-Schechter formalism then allows to obtain the number density of haloes considering that the gravitational collapse is a self-similar process, and thus, a given halo collapses if its mass scale variance surpasses a certain theshold for collapse at that redshift, and the probability that a halo has the required mass is distributed gaussianly with the variance corresponding to the associated mass.

The second hierarchy in density enhancements are the substructures embedded in a particular halo. As the gravitational collapse is a self-similar process, each halo will be the end node (the trunk) of an inverted halo merger tree at that redshift (Springel et al. 2005). As the DM is non-collisional, it relaxes much slower than normal matter, because it cannot radiate away energy to fall to the bottom of the gravitational potential well. Also, as friction is negligible, the angular momentum barrier will make the DM subhaloes to acquire stable orbits around the center of mass, but these subhaloes will retain their identities. Thus, inside each DM halo, it is expected that the full hierarchy of DM haloes is nested within, until the lowest mass haloes that formed. The number density of these subhaloes can be measured in Milky-Way sized halo simulations, and by approximating their abundance by a power-law behaviour (Via Lactea II simulation (Diemand et al. 2008), Acquarius project simulation (Springel et al. 2008)).

Apart from the number density of haloes and subhaloes, it is important to quantify the form of the density distribution within a particular structure, in order to compute the annihilation power output. Navarro, Frenk & White (1997), when studying the clustering of DM in N-body simulations, found that haloes from different Cold Dark Matter cosmologies all have the same universal density profile (the NFW profile). This profile is characterized by two parameters, the scale radius and the scale density, and this parameters can be (on average) regarded as a function of the halo mass and the redshift. Also, this DM density profile may be further enhanced by the gravitational effect of baryons on DM through adiabatic compression (see, for example Sellwood & McGaugh (2005); and Natarajan, Croton & Bertone (2008)). Thus, the total resulting DM distribution in the universe can be computed at a particular redshift.

Knowing the global DM distribution, one can compute the resulting energy output per baryon, which can be further compared with what can be obtained assuming a perfectly homogeneous DM distribution (see Mapelli, Ferrara & Pierpaoli (2006); and Cumberbatch, Lattanzi & Silk (2010)). One can also compute the energy generated per unit time by a particular halo of a given mass and redshift, and one can calculate what is the energy received by a particular halo due to the rest of the universe.

This additional energy injection may have interesting effects on the global IGM, as well as on the environment within particular DM haloes. For example, several authors (for example Cumberbatch, Lattanzi & Silk (2010); Mapelli, Ferrara & Pierpaoli (2006); Ripamonti, Mapelli & Ferrara (2007); Valdés et al. (2007); Pierpaoli (2004) and Natarajan & Schwarz (2009)) have studied the effects of DM annihilation (and also decays, in different DM models) on the IGM temperature and on the global ionization fraction. This extra heating may be detectable through the global 21 cm differential brightness temperature, measurable in the MHz frequency range. This differential brightness temperature arises as a result of the coupling of the neutral hydrogen spin temperature (that accounts for the hyperfine transition) to the IGM kinetic temperature, thus causing a difference between the spin temperature and the CMB temperature. Also, the energy input may contribute as an extra heating mechanism within haloes that can add up to the standard SNe and AGN feedback mechanisms (Natarajan, Croton & Bertone (2008)), and may change the temperature of the halo environment.

Regarding the observational evidence for the energy injection due to DM annihilations, no definite conclusion has been drawn yet. However, different observations of anomalous enhancements in detected signals from high-energy phenomena in the galactic halo and in the cosmic background suggest its presence. These signals correspond mainly to gamma ray detections (Fermi (Abdo et al. 2009), H.E.S.S (Aharonian et al. 2008) and EGRET (Sreekumar et al. 1998) experiments) and to measurements of cosmic ray positron fractions (PAMELA (Adriani et al. 2009) experiment). For example, Cline, Vincent & Xue (2010) and Finkbeiner et al. (2010) analyse the data sets by PAMELA, Fermi and H.E.S.S., and conclude that the observed signals could be accounted for by a $\sim 1TeV$ WIMP. They also find an enhanced interaction cross-section (see Sommerfeld enhancement, Section 4.5) for the annihilation process ($\sim 10^2$ times the thermal relic WIMP value). A similar result was also obtained by Elsässer & Mannheim (2004) with respect to the EGRET gamma ray data (Sreekumar et al. 1998). However, there is some debate regarding the compatibility of the presence of Sommerfeld enhancement with the non-detection of gamma ray flux from known DM structures (like galaxy clusters). In this line, the study by Pinzke, Pfrommer & Bergstrom (2009) determines that the attempts of explaining the Fermi, PAMELA and H.E.S.S. combined data with $\sim 1TeV$ WIMPS and cross sections enhanced by factors of $10^2 - 10^3$, are incompatible with the EGRET upper limits on the gamma ray emission from the Virgo galaxy cluster. Regarding the Fermi gamma ray excess, Hooper & Goodenough (2010) argue that it can be well accounted for by non-exotic processes (decaying pions, inverse Compton, point sources, etc...), except within 1.25° ($\approx 175pc$) from the galactic center, where the gamma ray excess is consistent with the prediction of a cusped ($\rho \propto r^{-1.34}$) DM density profile, and annihilating WIMPS with a thermal relic cross-section (no Sommerfeld enhancement) and masses in the range $m_\chi = 7.3 - 9.2GeV$. Also, Hooper, Finkbeiner & Dobler (2007) found that the excess microwave radiation within 20° from the galactic center, found by the WMAP experiment and called the WMAP Haze, can be well explained by a cusped DM profile with $\rho \propto r^{-1.2}$ in the inner kiloparsecs, and a WIMP with mass in the $100GeV$ to multi-TeV range and thermal relic cross section. It can be seen that no clear consensus exists neither on the significance of the results as positive indirect detections of DM, nor on the importance of these detections for discriminating among different WIMP scenarios. What can be said nonetheless, is that evidence of possible new exotic physics is accumulating, and that WIMP DM annihilation represents a well motivated option. As for the evidence for Sommerfeld enhancement, it is specially controversial and largely model-dependent. However, the DM annihilation interpretation of the observational evidence supports WIMP masses in the range $\sim 10GeV$ and $\sim 1TeV$.

The main goal of this work is to compute this additional energy injection, both locally within haloes and globally, and to asses the importance of this injection on the different processes mentioned above. All the computations will be done considering a cosmology consistent with the First Year Data Release of WMAP (Spergel et al. 2003). In particular, we will use $h = 0.72$, $\Omega_{m,0} = 0.27$, $\Omega_{\Lambda,0} = 0.73$, $f_{bary} \equiv \frac{\Omega_{b,0}}{\Omega_{m,0}} = 0.17$, $n_s = 0.99$ and $\sigma_8 = 0.9$. The paper is organized as follows. In Section 2, the thermal relic WIMP, and the two above mentioned well motivated particular DM models will be explained in greater detail. In Section 3, the statistics of the DM clustering on all hierarchies will be developed and the NFW universal density profile, as well as the adiabatic compression mechanism will be explained. In Section 4, the DM annihilation energy output, both globally (per baryon) and locally within a particular DM halo will be computed. Also, the clumpiness factor, defined as the ratio of output between the smoothed and fully clumped cases, will be calculated. In Section 5, the energy injected on the medium of a particular halo, due to the contribution of the rest of the universe, will be obtained for different cosmological scenarios. In Section 6, the effects of the annihilation energy injection on the global IGM will be followed in detail, computing the IGM temperature, the ionization fraction and the resulting 21 cm differential brightness temperature in this scenario. In Section 7, the formalism for calculating the effects of the DM annihilation energy injection on individual halos, in particular the change in temperature and ionization fraction of the intra halo medium (ICM for cluster-sized haloes), will be outlined. The general conclusions will be presented in Section 8.

2 WIMP MODELS AND THE THERMAL RELIC

As was previously mentioned in the introduction, the WIMP is a theorized particle that allows to account for the missing mass in the universe. The evidence of this missing mass is (as previously mentioned) mainly gravitational. This missing mass cannot come however from normal baryonic matter, because current Big-Bang nucleosynthesis constraints, like for example the primordial Helium abundance (Section 10.4 of Ryden (2003)), set stringent limits on the normal matter content.

For a certain particle, motivated by some beyond-standard physical scenario, to be a viable WIMP candidate, it must have some basic properties. For example, it has to be charge-neutral and it can interact only weakly with ordinary matter. Also, it has to be collisionless and massive in order to behave as Cold Dark Matter. A light DM particle will behave as Warm or Hot dark matter depending on if it was relativistic or not at the time of decoupling and also depending on its free streaming length (Angulo & White 2010), and the resulting structure formation scenario or minimum halo mass will be different to the CDM case. Also, a WIMP must be stable, or have a decay time longer than (or at least comparable to) the present Hubble time.

In some well motivated physical scenarios, the WIMP is a thermal relic. This means, as was mentioned before, that its creation and annihilation reaction were in thermal equilibrium with the radiation background in the early universe. Then, as the universe cooled down, the annihilation reaction was increasingly favoured over the creation reaction due to the rest-mass energy difference between both states. Finally, as the expansion rate of the universe became larger than the annihilation reaction rate, the global abundance of DM (its comoving number density) was frozen, and the probability of occurrence of an annihilation event became negligible.

In two well studied scenarios, the WIMP particles are such that they are their own anti-particle. For example in the case of a Kaluza-Klein excited state, arising naturally in compactified extra-dimensional models (like Universal Extra Dimensions or UED, in which all particles are able to propagate in the extra dimension provided they have enough energy), the WIMP is the lightest neutral gauge boson excited state, corresponding to the first excited state of the B boson or $B^{(1)}$, and as the standard model B boson, it is its own antiparticle (the B boson is a superposition of the photon of Quantum Electrodynamics and the Z boson of the weak interaction). Also, in the case of the MSSM (the minimal supersymetric standard model), considering conserved R-parity (and thus that superpartners are forbidden to decay to standard model particles), the WIMP is the lightest neutralino (i.e., the lightest mass eigenstate of the fermionic superpartners of the gauge bosons and the Higgses), and it is a Majorana fermion, and thus it is its own antiparticle.

In both these scenarios, the annihilation cross section is dependent only on the present day abundance of DM. This fact has been dubbed the WIMP miracle and is explained in what follows. Also, both scenarios are explained in greater detail.

2.1 The WIMP miracle

The WIMP miracle refers to the fact that, given that the WIMP is a thermal relic, its creation/annihilation cross section can be computed without needing extra model-dependent input (except for the fact that the cross section must not depend on the energy of the WIMP, i.e., the s-wave cross section must be dominant). The cross section then only depends on the present day DM density parameter $\Omega_{m,0}$, and the present day value of the Hubble parameter h (that gives the current expansion rate).

Intuitively, one would think that a higher cross section $< \sigma v >$ would lead to less relic abundance of DM, thus resulting in a smaller value of $\Omega_{m,0}$. Both quantities are, indeed, inversely proportional to each other.

Obtaining this cross section is a standard derivation and it is done in, for example, Section 5.2 of Kolb & Turner (1990). For the value of the cross section, Hooper, Finkbeiner & Dobler (2007) use $< \sigma v >= 3 \times 10^{-26} [cm^3/s]$, and in the cosmology used in this work, that gives:

$$< \sigma v >= \frac{4 \times 10^{-27}}{\Omega_{\chi,0} h^2} [cm^3/s]. \quad (1)$$

In all that follows, we will use that value for the cross section of WIMP annihilation.

Now we will motivate and explain two scenarios that give rise naturally to a thermal relic WIMP with the above-given cross section.

2.2 The KK DM particle

In extra dimensional models (i.e., physical models that are built considering more than three spatial dimensions), the additional spatial degrees of freedom may be accessible to all or some of the particles. Also, these additional dimensions may be compactified differently and on different energy scales. If a standard model particle can propagate in this compactified (and thus finitely extended) dimensions, they will appear more massive in the four dimensional effective theory. In some cases, these excited states of standard model particles may have the desirable features of the WIMP. Here we will briefly discuss the lightest KK particle WIMP candidate and the extra-dimensional scenario in which it arises. We loosely follow the excellent review by Hooper & Profumo (2007).

The first one to seriously propose that there may be more spatial dimensions was Theodor Kaluza (Kaluza 1921), in an attempt to explain electromagnetism in the framework of General Relativity. Although this proposal was not considered by mainstream physics, recently it was demonstrated that string theory could not be formulated in only four dimensions, and thus, this idea was again taken into account.

One extra dimensional scenario that is interesting for being able to provide a suitable DM particle is Universal Extra Dimensions (UED). In this scenario, proposed by Appelquist et al. (2001), all standard model (SM) particles are able to propagate in the extra dimension. Because this dimension is compactified, and thus has a finite extent, the momentum that a particle can acquire in it will be discreet (the idea is similar to that of an electron propagating in a box of given size), thus giving an apparent extra rest-mass in the four dimensional world.

The spectra of different possible momentum states in the extra dimension will give a series of possible masses of a particle, quantized by the number of the excitation state. This masses will depend on the radius of compactification and will be given roughly by:

$$m^2_{X^{(n)}} = \frac{n^2}{R^2} + m^2_{X^{(0)}}, \qquad (2)$$

where $m_{X^{(n)}}$ is the mass of the n^{th} excited Kaluza-Klein state of a SM particle X, $m_{X^{(0)}}$ is its mass in the SM and R is the compactification radius of the extra dimension, given in natural units (so it has dimension of $Energy^{-1}$). Then, the KK particles are the same SM particles, but considering their excitations in the extra dimension. Interactions between SM particles and KK particles are possible, but are suppressed (thus, these particles are weakly interacting). Moreover, the lightest KK particle is stable because of conservation of momentum in the extra dimension.

As was already mentioned, the lightest KK particle in the UED framework is the $B^{(1)}$, i.e., the first KK excited state of the B gauge boson (also called the KK-photon). This particle is charge neutral, and can annihilate with itself, and thus is a suitable WIMP candidate.

Some of the ways in which KK particles can interact with SM particles are through decays, annihilations and scatterings. For example, a heavier KK particle can decay into a lighter KK particle emitting standard model particles, until it has cascaded into the $B^{(1)}$ (also called γ_1, see Figure 4 of Hooper & Profumo (2007)).

Also, more interestingly in view of the possible effects of WIMP annihilation on the IGM, two $B^{(1)}$s can annihilate to lepton pairs and photons (see Figure 16 of Hooper & Profumo (2007)).

Finally, the KK-particles and in particular, the $B^{(1)}$, can scatter off SM quarks and leptons (see Figures 10 and 12 of Hooper & Profumo (2007)). Although, these processes are highly suppressed (making the $B^{(1)}$ a weakly interacting particle), they can occur, and so, this WIMP candidate can be searched for using direct detection methods (for example, scatterings off heavy nuclei).

Although of importance for particle physics and for constraining the UED parameters in collision experiments, a computation of the branching ratios and cross sections of the processes is beyond the scope of this work, and it is also not required for the computations performed in this work, because the resulting WIMP is a thermal relic.

2.3 The Neutralino

For this section, we will follow two reviews that analyse different theoretical aspects of the SUSY neutralino. The first review, by Martin (2008), gives a thorough introduction to the MSSM, defining what is supersymmetry, giving the MSSM lagrangian, explaining the different SUSY-breaking scenarios (that ultimately fix the parameters of the particular model), etc... The second review, by Jungman, Kamionkowski & Griest (1996), treats the neutralino DM WIMP candidate, and its associated physical features, with in-depth detail, calculating the particular cross sections of all the interaction channels of the neutralino with SM particles for the most common SUSY scenarios.

Supersymmetry is a particular symmetry property of the lagrangian of a physical theory, such that said lagrangian remains invariant if a supersymetric transformation is performed on the fields of the theory. The supersymmetric transformation is such that the change in a fermionic field is a bosonic field, and the change in a bosonic field is a fermionic filed. As in quantum field theory, the fields represent different particle contents (the particles are nothing more than the excited states of the fields), a supersymmetric theory naturally has one boson for each fermion present, and vice-versa.

The lagrangian of the SM of particle physics is not supersymmetric. As the SM has been remarkably successful in accounting for all known physical interactions (except for gravity), a natural question is why would it be needed to propose a supersymmetric theory. As of today, the two main motivations for invoking supersymmetry (SUSY) are the unification of the interaction coupling constants at high energy and the solution of the hierarchy problem.

It is a known fact in quantum field theory, that the coupling constants are a function of the energy (or momentum) of the interaction. This is called the running of the couplings and it is a consequence of the infinite loop contributions to any given process. Although a more detailed explanation of this phenomena is beyond the scope of this work, it is sufficient to say that by using renormalisation techniques, it is possible to find the dependence of the couplings with the energy, and that when considering SUSY, the couplings tend to unify at an energy scale of $10^{16} GeV$ (see Figure 5.8 of Martin (2008)).

The strong hierarchy problem comes from the quantum corrections to the lagrangian mass of the Higgs field in the standard model. What happens is that for every particle in the model, the Higgs mass receives a correction that is linear on the energy scale at which the SM ceases to be valid. Of course, if the SM is the ultimate physical theory, then this would not be a problem, however, this cannot be because the SM does not explain gravity. Reasonable order of magnitude arguments point in the direction that, at least at an energy scale of the order of the Planck Mass (M_p), quantum-gravitational effects should be important (for example, the fact that for a particle of mass M_p, its Compton wavelength is comparable to its Schwarzschild radius), and so, the SM ceases to be valid at least at this energy scale. SUSY naturally solves this problem, because the contribution to the Higgs mass is positive in the case of bosons and negative in the case of fermions, and so as for each boson there is a fermion, the contribution cancels out exactly.

The particle content of the MSSM (the Minimal Supersymmetric Standard Model) is the same as that of the SM, but for every SM particle, there is an associated supersymmetric partner (also, the Higgs field is different from the one in the SM, being two fields instead of just one). The naming scheme for the superpartners is to maintain the root of the name of the SM particle, but to change the end of the name with the suffix -ino in the case of fermionic superpartners of SM bosons and to add the prefix s- in the case of bosonic (scalar) superpartners of SM fermions. For example, the superpartners of the electron and the muon are the selectron and the smuon, and the superpartners of the photon and the Z boson are the photino and the Zino.

As it was mentioned above, the WIMP candidate of SUSY is the lightest neutralino (unless the gravitino, the superpartner of the graviton in supergravity is lighter than the neutralino, but this scenario will not be considered here). The neutralinos are the mass eigenstates of the superpartners of the neutral gauge bosons and the Higgses, i.e., the Bino ($\tilde{B}$), neutral Wino ($\tilde{W}^0$) and the neutral Higgsinos ($\tilde{H}_d^0$ and $\tilde{H}_u^0$). They are labelled $\tilde{N}_i, i = 1...4$ in order of increasing mass, such that the $\tilde{N}_1$ corresponds to the lightest neutralino. The $\tilde{N}_1$, (the WIMP candidate) will be in general a linear combination of the gauginos (Bino and Wino) and the Higgsinos, and it will have a somewhat different phenomenology depending on its specific particle mixture. Although the precise differences between a mainly gaugino, mainly Higgsino or mixed gaugino-Higgsino type neutralino are beyond the scope of this work, it is sufficient to mention that, in general (in order to give the appropriate above-mentioned interaction cross section), a mixed gaugino-Higgsino composition is assumed.

In R-parity conserving SUSY scenarios, no superpartner can decay to SM particles only (SM particles have different R-parity than superpartners), and so the lightest neutralino ($\tilde{N}_1$) will be stable, whereas more massive SUSY particles can decay into the $\tilde{N}_1$ emitting standard model particles (as long as the standard conservation rules are not violated). Also, the ($\tilde{N}_1$) is a Majorana fermion, and thus it can self-annihilate into SM particles. The SUSY particles can also interact (scatter off) standard model particles, but these scatterings are suppressed, thus the $\tilde{N}_1$ is weakly interacting. The main annihilation processes of neutralino into SM particles is into fermion pairs, although it can also annihilate into gauge bosons (W and Z) at tree-level. At 1-loop level, the neutralino can annihilate directly into gluons or photons, and although this is greatly suppressed compared to tree-level processes, the direct decay into photons is important because it signals a smoking gun of annihilation (the resulting two photons will have an energy very close to the neutralino rest-mass energy, and so it is a clear signal with no contaminants). The Feynman diagrams of the tree-level annihilation channels are shown in Figures 9, 10 and 16 of Jungman, Kamionkowski & Griest (1996).

Like in the case of the lightest KK particle, the Feynmann diagrams were included just to illustrate the available annihilation channels, and a computation of the precise cross sections for each process is beyond the scope of this work (although it is done explicitely by Jungman, Kamionkowski & Griest (1996)).

Finally, it is important to mention that the phenomenologies of KK particles (as they arise in UED) and of SUSY are very similar, and both of them could be tested, for example in particle colliders, by studying interactions above a certain energy scale. In the case of KK, this energy scale corresponds to the inverse of the radius of compactification of the extra dimmension, whereas in SUSY, it corresponds to the mass of the neutralinos and superpartners. Current collider lower limits on the mass scale of this new physics (for example the LHC limits) are on the order of the 100 GeV and increasing. This mass limit will motivate the values that we adopt for the WIMP mass in the rest of this work. We use both a WIMP mass of 10 GeV and of 1TeV.

3 THE DM CLUSTERING

In standard FRW (Friedmann-Robertson-Walker) cosmology, the universe is assumed to be homogeneous and isotropic on large scales. However, the matter is distributed in a random but not homogeneous manner on small scales, and thus the universe exhibits structure (like voids, clusters of galaxies, cosmic filaments, etc...). The hierarchical structure formation scenario is a natural consequence of the ΛCDM cosmology, and it predicts that the DM accretion is a clumped process. In this scenario, structures of all mass scales are allowed to collapse, and so the densest and smallest objects collapse first, corresponding to small peaks on top of larger peaks of the matter overdensity field. In order to account for the formation of large-scale structure, the DM needs to be followed in the gravitational collapse process, but considering the corresponding effect of Λ (the cosmological constant) on the background expansion.

There are two main approaches for following the gravitational collapse of the DM. The first approach is to substitute the continuous overdensity field by DM point masses and to perform computational N-body simulations of their mutual interactions. The second approach is to make use of the statistical properties of the overdensity field, and develop a formalism that allows to analytically compute the average clustering of the DM at different redshifts.

As it was mentioned in the Introduction, the gravitational collapse process is hierarchical and self-similar, and so different levels of clustering are expected. In the following subsections we explain the prescriptions adopted to account for the DM clustering at all these levels, considering also the distribution of DM within a particular halo or subhalo. In Section 3.1, we follow the analytic approach, using the Press-Schechter formalism (Press & Schechter (1974); Mo & White (1996); Bond et al. (1991); Sheth, Mo & Tormen (2001); Lacey & Cole (1993) among others) to compute the number density of DM haloes per decade in mass. In Section 3.2, we account for the presence of substructure by considering the substructure mass function given by Giocoli, Tormen & van den Bosch (2008). In Section 3.3, we present the universal NFW density profile (Navarro, Frenk & White 1997), that gives the DM distribution within each gravitationally bound halo, and explain how to calculate its parameters for different halo masses at different redshifts. Finally, in Section 3.4, we explain the effect that the gravitational collapse of the barionic matter (in particular, the formation of a supermassive black hole (SMBH)) can have on the DM density profile through adiabatic compression.

3.1 The halo mass function

The analytic approach to obtaining the clustering statistics of DM has been developed in time by different authors. It was in Press & Schechter (1974) where a formalism for computing the halo mass function was first obtained, starting from the power spectrum of matter density fluctuations. Later on, this formalism was refined by Bond et al. (1991), where it was cast in a more rigorous mathematical form (excursion set theory and random walks). Also, it was extended by Lacey & Cole (1993) for computing the halo merger rates at different redshifts, and also the average number of mergers a halo has undergone since its formation as a function of mass and redshift (they also give a prescription to generate montecarlo merger trees). A further extension of the formalism was done by Mo & White (1996), to compute the clustering statistics (correlation functions and bias) of haloes. Finally, Sheth, Mo & Tormen (2001) slightly modify this formalism (in particular, the functional form of the halo mass function) to account for ellipsoidal collapse due to the non-sphericity of overdensities (for a discussion of triaxiality of DM haloes, see Piffl & Sotnikova (2008)). We use this formalism, as presented in Mo & White (1996), but using the modified Sheth, Mo & Tormen (2001) halo mass function and bias factor, calibrated with the GIF simulations (Kauffmann et al. 1999).

We consider the overdensity $\delta(x)$ defined as $\delta(x) = \frac{\rho(x)-\bar{\rho}}{\bar{\rho}}$, and the overdensity threshold for collapse $\delta_c(z)$, defined as the density contrast (in the linear approximation) required for an overdensity in a certain region to already have formed a collapsed object (Navarro, Frenk & White (1997), equation A14). We consider also the mass fluctuation $\sigma(R)$, defined as the standard deviation of the matter overdensity field when smoothed on a scale of size R. Finally, the dimensionless mass parameter is defined as $\nu = \frac{\delta_c(z)}{\sigma(R(M,z))}$, and it is a measurement of the mass of a collapsed region (DM halo) relative to the mass of the structures that have recently collapsed at redshift z.

We will use the Sheth, Mo & Tormen (2001) probability distribution $f(\nu)$. The mass fluctuation $\sigma(R)$ is computed following Lacey & Cole (1993) and Mo & White (1996), starting from the power spectrum of matter overdensities, $P(k)$, at redshift z. When calculating the mass function we adopt a primordial power spectrum of the form $P(k) = Ak^{n_s}$, where A is a normalization. We use the WMAP1 (Spergel et al. (2003)) scalar index, $n_s = 0.99$.

The effects on the power spectrum due to the gravitational collapse of the DM on sub-horizon scales after the radiation-matter equality epoch and the Barion Acoustic Oscillations (BAOs) are encoded in the transfer function. We adopt the functional form given by Bardeen et al. (the BBKS transfer function), which ignores the BAOs.

3.2 The substructure mass function

The second level of clustering of the DM corresponds to the self-bounded haloes that retain their identity within bigger haloes. The presence of these substructures is a natural consequence of the hierarchical structure formation picture, because haloes at all redshifts are formed by the aggregation of smaller parent haloes. As the DM is collisionless, DM haloes are significantly less disrupted than barionic matter during the merging processes, and thus subhaloes may survive up to the smallest scales (due to the negligible, but nonzero, free-streaming of the WIMPS). Many authors (for example Kamionkowski, Koushiappas & Kuhlen (2010); Giocoli, Pieri, Tormen & Moreno (2009); Giocoli, Pieri & Tormen (2008); Taylor & Babul (2004); Pieri, Bertone & Branchini (2008)) have investigated the clustering properties of the subhaloes by means of fitting an analytic form to the subhalo mass function obtained in high-resolution numerical N-body simulations and re-simulations.

We use the substructure mass function proposed by Giocoli, Tormen & van den Bosch (2008), because it also considers the evolution of the substructure in time, due to the combined effects of gravitational heating and tidal stripping in the potential well of the main halo. These effects will tend to erode the subhaloes, which are the remnants of the haloes accreted by the host halo. As was found by these authors, the mass loss (to the smooth component of the main halo) of subhaloes can be approximated by an exponential decay of the subhalo mass on a characteristic timescale that is proportional to the dynamical time of the main halo.

Explicitly, the unevolved subhalo mass function (that considers all subhaloes with the mass they had when they were accreted) is universal, and is given by:

$$\frac{dN}{dln(m_v/M_0)} = N_0 x^{-\alpha} e^{-6.283x^3}, x = \frac{m_v}{\alpha M_0}, \quad (3)$$

with $\alpha = 0.8$ and $N_0 = 0.21$. These values were calibrated using the GIF Kauffmann et al. (1999) and GIF2 Gao et al. (2004) simmulations, as well as resimulations done by Dolag et al. (2005). Here, m_v represents the unevolved subhalo mass (the mass that the halo had when it was accreted) and M_0 represents the present-day host mass.

To account for time evolution, the authors find the following relation between the mass of a subhalo at time t (given that it was accreted at time t_m), and its unevolved mass:

$$m_{sb}(t) = m_v exp\left[-\frac{t-t_m}{\tau(z)}\right], \quad (4)$$

where m_{sb} is the evolved mass and $\tau(z)$ is the characteristic mass loss time, given by

$$\tau(z) = \tau_0 \left[\frac{\sigma(z, M_0)}{\sigma(z=0, M_0)}\right]^{-1/2} \left[\frac{H(z)}{H_0}\right]^{-1}, \quad (5)$$

and $\tau_0 = 2.0Gyr$.

In this work, it was useful to approximate the accretion time of all haloes by the time at which the main halo collapsed, corresponding to a redshift z_{coll}, which we take as the redshift at which it acquired half of its mass (see Section 3.3). In terms of the look-back time to redshift z ($LBT(z)$), equation 15 can be approximated by:

$$m_{sb} = m_v exp\left[-\frac{LBT(z_{coll}) - LBT(z)}{\tau(z)}\right]. \quad (6)$$

Now, the required subhalo mass function is the one that includes the mass loss of subhaloes in time, so it should be $\frac{dN}{dm_{sb}} = \frac{dN}{dm_v}\frac{dm_v}{dm_{sb}}$, using the chain rule. Expressing the subhalo mass function in terms of m_{sb} instead of m_v, one obtains:

$$\frac{dN}{dm} = \frac{N_0}{m} x^{-\alpha} e^{-6.283x^3}, x = \frac{mK^{-1}(z, M_h)}{\alpha M_h}, \tag{7}$$

where m is the present day (at redshift z), evolved mass of a subhalo, M_h is the mass of the host halo and K is defined by

$$K(z, M_h) = exp\left[-\frac{LBT(z_{coll}(M_h)) - LBT(z)}{\tau(z)}\right]. \tag{8}$$

It can be seen that the behaviour of the subhalo mass function is that of a power law with an exponential cutoff, and that all mass scales are displaced as a function of time since halo formation. The displacement is such that a present day subhalo of mass m, corresponded to a halo of greater mass (by a factor K), and so its abundance is decreased because it is the abundance corresponding to the greater mass at the time of halo formation.

These last two equations give the number of subhaloes present in a halo of mass M at redshift z, that have a mass between m and $m + dm$, and so correspond to the subhalo mass function that we need. In the next section, we explore the smooth density profile of a particular halo, in order to account for the last level of the DM clustering hierarchy.

3.3 The NFW universal density profile

The last hierarchy corresponds to how the DM is smoothly distributed within a particular halo or subhalo. This DM distribution appears to be universal, as found by Navarro, Frenk & White (1997) using N-body simulations, and is given by the NFW density profile:

$$\rho(r) = \frac{\rho_0}{(r/r_s)(1 + r/r_s)^2}, \tag{9}$$

where ρ_0 is the characteristic density and r_s is the scale radius. Thus, the NFW profile depends on only two parameters, which on average only depend on the mass of a halo and the redshift at which it is observed. Before obtaining these parameters, it will be necessary to compute the redshift at which a halo that currently (at redshift z) has a mass M was formed.

For this quantity Navarro, Frenk & White (1997) use the redshift at which a halo which currently (at redshift z) has a mass M has just acquired half of its mass. The authors make use of the gaussianity of the overdensity field to compute the redshift of collapse as:

$$erfc\left(\frac{\delta_c(z_{coll}(M, z)) - \delta_c(z)}{2\left[\sigma^2(0.01M, z) - \sigma^2(M, z)\right]}\right) = 1/2. \tag{10}$$

The interpretation of this expression is that, if we consider a halo of mass M at redshift z, $z_{coll}(M, z)$ will correspond to the redshift at which a collapsed substructure of mass $0.01M$ was already part of the halo under consideration with a probability of 1/2. The above equation is an implicit definition of $z_{coll}(M, z)$, and the election of the mass of the small substructure (of $0.01M$) is motivated by comparisons to N-body simulations considered by the authors.

With the obtained $z_{coll}(M, z)$, we proceed to determine ρ_0 and r_s using the following relations:

$$\rho_0 = \rho_{crit}(z)\delta_0(M, z), \tag{11}$$

where $\rho_{crit}(z)$ is the critical density of the universe at redshift z, and $\delta_0(M, z)$ is a characteristic overdensity (or density contrast) that depends on the mass and redshift of the halo whose NFW profile we want to obtain.

Also,

$$r_s = \frac{r_{vir}(M, z)}{c(M, z)}, \tag{12}$$

where $r_{vir}(M, z)$ is the virial radius of a halo of mass M at redshift z, corresponding the the radius at which the average density within is equal to the density required for the halo to be a self-gravitating virialized structure (in the case of the Einstein-De Sitter cosmology, this density is 200 times the mean density of the universe). $c(M, z)$ is the concentration parameter of the halo.

The virial radius is given by Navarro, Frenk & White (1997) as:

$$r_{vir}(M, z) = 1.63 \times 10^{-2} \left(\frac{M}{h^{-1}M_\odot}\right)^{1/3} \times$$
$$\times \left[\frac{\Omega_{m,0}}{\Omega_m(z)}\right]^{-1/3} (1 + z)^{-1} h^{-1} kpc, \tag{13}$$

where $\Omega_m(z)$ is the matter density parameter at redshift z, and the virial radius is given in proper kpc.

The characteristic density is given by:

$$\delta_0 = 3.41 \times 10^3 \Omega_m(z) \left(\frac{1 + z_{coll}(M, z)}{1 + z}\right)^3. \tag{14}$$

Finally, the concentration parameter is implicitly given in terms of the characteristic density contrast by the relation:

$$\delta_0(M, z) = \frac{200}{3} \frac{c^3(M, z)}{\left[ln(1 + c(M, z)) - \frac{c(M,z)}{(1+c(M,z))}\right]}. \tag{15}$$

Thus, the density profile of a particular halo or subhalo is, on average, completely specified by its mass and redshift.

In the next section, we proceed to study the consequences of the collapse of the baryons on the density profile of the DM haloes, and obtain a modified density profile for the latter considering the growth of a central SMBH, a process that appears to be ubiquitous in galaxy formation.

3.4 Adiabatic compression

We consider the modification in the NFW DM density profile resulting from the gravitational collapse of baryons. Baryons behave dynamically differently from DM in their collapse process because they can heat and radiate away their energy, as they are not collisionless and have nonzero internal pressure. Thus, as they lose energy, they fall towards the center of the gravitational potential well (this process is also called baryonic infall or cooling). This is the main mechanism that allows the formation of galaxies within the DM haloes, and it is also responsible for the adiabatic compression of the DM halo density profile.

Different authors have studied the adiabatic compression mechanism, and have given algorithms to compute the compressed DM density profile, given the original, uncompressed profile and the newly grown density profile of the collapsed baryonic component. Two of the most used methods are the Blumenthal algorithm (Blumenthal 1984) and the Young algorithm (Young 1980). The Young algorithm assumes that the potential well has spherical symmetry, and so it corresponds to a central potential problem. The Blumenthal algorithm further assumes that all the orbits of the DM particles are circular. Sellwood & McGaugh (2005) conclude that the Blumenthal algorithm overpredicts the compression in the inner regions.

We use a different algorithm and account only for the adiabatic compression due to the formation of a point mass (i.e., a SMBH) in the center of the potential well. We implement this algorithm as described in Natarajan, Croton & Bertone (2008).

This algorithm assumes that the density profile is of the initial NFW form up to the radius of gravitational influence of the SMBH (defined as the radius up to which it is the main contributor to the contained mass), and that within this radius, the density profile is described by a power-law with a different (steeper) exponent. It also assumes (like the Blumenthal algorithm), that the original orbits of DM particles in the NFW profile were circular.

According to Natarajan, Croton & Bertone (2008), the value of the exponent of the density profile in the inner region is given by

$$\gamma_{spike} = 2 + \frac{1}{4-\gamma}. \tag{16}$$

The derivation of the value of the exponent can be found in Quinlan, Hernquist & Sigurdsson (1995).

Finally, we need the maximum density and the radius of gravitational influence of the BH to have the complete density profile. For the maximum density, we use:

$$\rho_{DM}^{max} = \frac{m_\chi}{t_{spike} < \sigma v >}, \tag{17}$$

where m_χ is the mass of the WIMP particle, and $< \sigma v >$ is the thermal relic annihilation cross-section (see Section 2.1). For t_{spike}, the time elapsed since the spike was formed, we use $t_{spike} = LBT(z_{coll})$, i.e., the look-back time to the redshift at which the halo collapsed (calculated as mentioned in Section 3.3).

For the gravitational influence radius of the black hole, we use:

$$r_{BH} = 0.2\frac{GM_{BH}}{\sigma_{sph}^2}, \tag{18}$$

where M_{BH} is the black hole mass, and σ_{sph} is the velocity dispersion of the spheroid component (the bulge in the case of haloes typical of late type galaxies).

For σ_{sph}, we use the observational relation between spheroid velocity dispersion and BH mass, as presented in Murray, Quataert & Thompson (2005):

$$M_{BH} = 1.5 \times 10^8 \left(\frac{\sigma_{sph}}{200[km/s]}\right)^4 M_\odot. \tag{19}$$

The mass of the black hole depends, on average, only on the mass of the host halo and on the fact that the host is a main halo or a subhalo. The relation between both masses is given by (Lagos, Cora & Padilla 2008):

$$log\left(\frac{M_{BH}}{M_\odot}\right) = 0.84 log\left(\frac{M_{halo}}{M_\odot}\right) - 2.1 \tag{20}$$

for the case of a main halo, and

$$log\left(\frac{M_{BH}}{M_\odot}\right) = 0.84 log\left(\frac{M_{halo}}{M_\odot}\right) - 2.9 \tag{21}$$

for the case of a subhalo.

Now we have all the ingredients for computing the adiabatically compressed DM density profile for a given halo of mass M at redshift z.

Putting all the pieces together, the adiabatically compressed density profile of a halo has four different regimes, and is given by:

$$\rho_{DM}(r) = \rho_{NFW}(r), r > r_{BH}, \tag{22}$$

$$\rho_{DM}(r) = \rho_{NFW}(r_{BH})\left(\frac{r}{r_{BH}}\right)^{-\gamma_{spike}}, r_{plateau} < r < r_{BH}, \tag{23}$$

$$\rho_{DM}(r) = \frac{m_\chi}{t_{spike} < \sigma v >}, 4r_s < r < r_{plateau}, \tag{24}$$

$$\rho_{DM}(r) = 0, r < 4r_s, \tag{25}$$

where $r_{plateau}$ is the radius at which the density of the spike equals the maximum attainable DM density, and r_s is the Schwarzschild radius of the BH. In Figure 1, we show the adiabatically compressed density profile of a DM halo of mass $5 \times 10^{13} M_\odot$ at redshift $z = 1$ (Typical of QSO systems). The four regimes are clearly distinguishable. The outer slope corresponds to the NFW $\gamma = 1$ and the inner slope corresponds to $\gamma_{spike} = \frac{7}{3}$.

4 DM ANNIHILATION ENERGY OUTPUT

Having considered the clustering properties of the DM at all scales and hierarchy levels, and having explained two particular DM WIMP candidates, motivating their expected masses and annihilation cross-sections, we can proceed to compute the expected energy output of annihilations in local structures (halos) and as an average for the whole IGM. In this section, we obtain the luminosity due to annihilations of individual DM haloes, considering the clustering analysed previously, and we also compute the annihilation energy rate injected to the IGM, per baryon, in the universe as a whole.

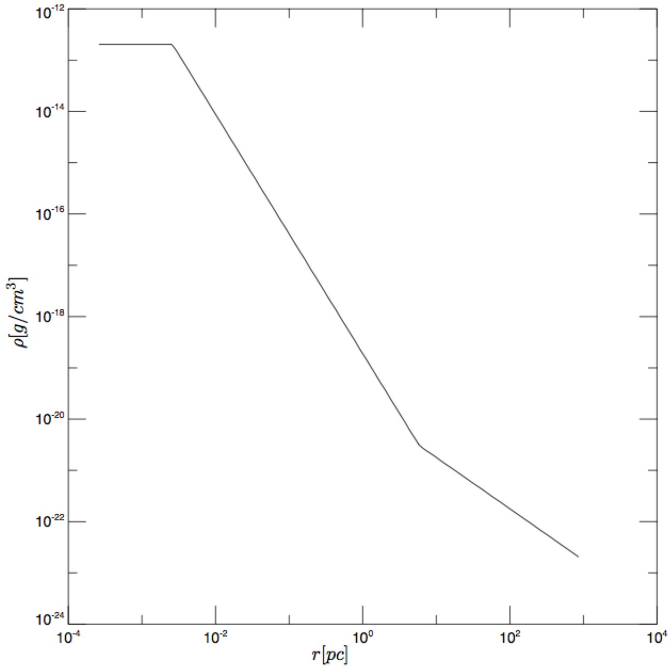

Figure 1. The adiabatically compressed density profile of a halo with mass $5 \times 10^{13} M_\odot$, at redshift $z = 1$.

We also mention the observational evidence of this annihilation energy injection process in satellite haloes and in the Milky Way (MW). Finally, we asses the importance of the DM clumpiness in the energy output, comparing the case of a perfectly smooth universe with one with clustered DM.

First, let us consider the generic energy output. The reaction rate of the annihilation process is given by

$$\Gamma = n_\chi < \sigma v >, \tag{26}$$

and thus, the variation of the number density of WIMPS can be calculated as:

$$\frac{dn}{dt} = \frac{1}{2} n_\chi^2 < \sigma v > . \tag{27}$$

As in the annihilation process the WIMPS are destroyed, we can consider that all their rest-mass is available as part of the energy output (actually, only a fraction of this energy will be available for affecting the environment, depending on the mechanism that couples the annihilation products and the IGM or halo medium). Then, the power density of the energy output can be written as:

$$\epsilon_\chi = \frac{1}{2} m_\chi c^2 n_\chi^2 < \sigma v > . \tag{28}$$

This equation is completely general, and so it applies for haloes and also for the diffuse IGM. Let us now consider the power output in the different situations (we will call them local and global).

4.1 The smooth DM annihilation energy injection rate per baryon

First we consider the global case, assuming a perfectly smooth DM density. This case is treated, for example, by Mapelli, Ferrara & Pierpaoli (2006); Ripamonti, Mapelli & Ferrara (2007); and Cumberbatch, Lattanzi & Silk (2010). As the universe may be infinite in spatial extent (as would be the case for flat, i.e. ΛCDM and Einstein-De Sitter, and Open cosmologies), the relevant quantity is the energy injected to the IGM per baryon. In terms of the present day WIMP number density, this is calculated as:

$$\dot{E}_\chi^{smooth} = \frac{1}{2} \frac{m_\chi}{n_{b,0}} c^2 n_{\chi,0}^2 (1+z)^3 < \sigma v > f_{abs}(z), \tag{29}$$

where $n_{\chi,0}$ is the present day DM number density, and is calculated as

$$n_{\chi,0} = \Omega_{dm,0} \frac{\rho_{c,0}}{m_\chi}, \tag{30}$$

where $\Omega_{dm,0} = (1 - f_{bary})\Omega_{m,0}$ is the present day DM density parameter, $\rho_{c,0}$ is the present day critical density of the universe and m_χ is the WIMP mass. Also, $n_{b,0}$ is the present day baryon density, and is calculated as

$$n_{b,0} = \Omega_{b,0} \frac{\rho_{c,0}}{\mu m_H}, \tag{31}$$

where $\Omega_{b,0}$ is the present day baryonic density parameter (equal to $f_{bary}\Omega_{m,0}$), m_H is the hydrogen mass and μ is the mean atomic weight of the baryon content. The mean atomic weight, considering a universe with only hydrogen and helium (a good approximation, particularly before star formation), can be computed as $\mu = f_H + 4 f_{He}$, where f_H is the fraction of hydrogen and f_{He} is the fraction of helium by number. Assuming a value of $X = 0.74$ and $Y = 0.26$ (the hydrogen and helium fractions by mass, respectively), gives $f_H = 0.92$ and $f_{He} = 0.08$. Thus, $\mu = 1.24$ will be used in this work.

Knowing the absorption fraction of the energy $f_{abs}(z)$, we can readily compute the energy injected to the IGM per baryon through DM annihilations. Different authors use various prescriptions for $f_{abs}(z)$. Natarajan & Schwarz (2009) consider that only the photons resulting as secondary annihilation products can inject energy to the IGM, and calculate the photon energy spectrum for different neutralino models explicitly. They consider that as the photons propagate, they loose energy, and compute the probability that they scatter off the IGM atoms. They find that $f_{abs}(z)$ is in the range of $0.1 - 0.2$ for $z < 50$ (they do not consider higher redshifts).

Cumberbatch, Lattanzi & Silk (2010), compute $f_{abs}(z)$ for the neutralino (see also (Ripamonti, Mapelli & Ferrara 2007)), calculating first the number of photons and electrons produced per neutralino annihilation event, and they obtain $f_{abs}(z)$ in the range of $0.01 - 0.1$, being higher for higher z (and considering redshifts up to $z = 1500$).

Other authors, like Mapelli, Ferrara & Pierpaoli (2006), simply assume that $f_{abs}(z) = 1$, and compute the maximal effects that their WIMP candidates can have on the IGM. We will consider that f_{abs} is a constant that does de-

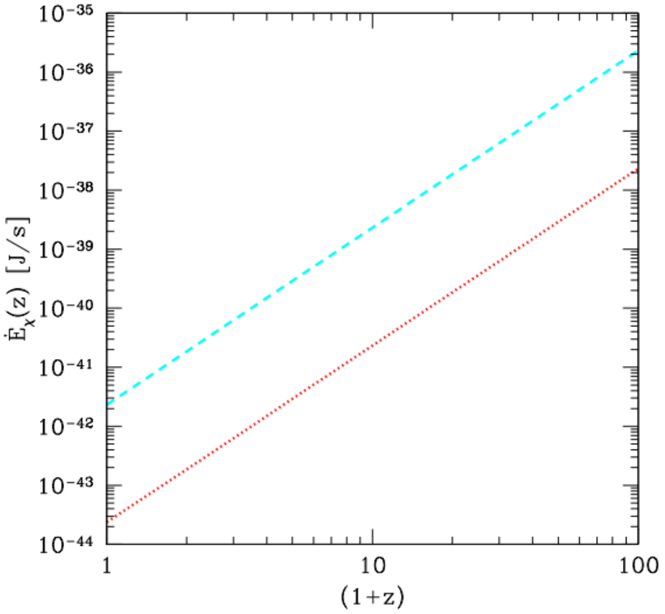

Figure 2. The smooth energy injection rate per baryon $\dot{E}_\chi(z)$, for different WIMP masses. The dotted curve corresponds to a WIMP mass of 1TeV and the dashed curve to a WIMP mass of 10GeV.

pend on redshift, and we will use the values $f_{abs} = 0.01$, 0.1 and 1, in order to obtain results comparable to the different authors.

In Figure 2, we show the results obtained for the smooth energy injection per baryon, for two different WIMP masses (1TeV and 10GeV), as explained in the caption. We only consider the maximal absorption fraction ($f_{abs} = 1$), because for other values, the resulting curves should simply be rescaled by f_{abs}. It can be seen that the effect of a lower WIMP mass is, as expected, to boost the energy injection rate by a factor $\propto m_\chi^{-1}$.

4.2 The DM annihilation luminosity of a halo

Having considered the global case of the energy injection to the IGM, we now consider the energy output per unit time (or luminosity) of a particular halo of mass M at redshift z. Following Natarajan, Croton & Bertone (2008), from the general formula the energy output integrated on the volume of the halo is given by

$$L_\chi = \frac{<\sigma v> c^2}{2m_\chi} \int_V \rho^2_{DM}(x,t) d^3x, \qquad (32)$$

where ρ_{DM} is the complete DM density profile of the halo, accounting for the smooth main halo, the substructure and the adiabatic compression in both (see Section 3.2 - Section 3.4). This luminosity can be decomposed into the main halo luminosity and the substructure luminosity such that:

$$L_\chi = L_{\chi,main} + L_{\chi,subs}, \qquad (33)$$

where

$$\begin{aligned} L_{\chi,main} &= L_\chi(M_{main}, z) = \\ &= \frac{<\sigma v> c^2}{2m_\chi} \int_V \rho^2_{DM}(r, M_{main}, z) dV, \end{aligned} \qquad (34)$$

and

$$L_{\chi,subs} = L_{\chi,subs}(M_{main}, z) = \int_{m_{free}}^{M_{main}} \frac{dN}{dm} L_\chi(m,z) dm. \qquad (35)$$

Note that in the above equations, $L_\chi(M,z)$ is the DM annihilation luminosity of a smooth, adiabatically compressed halo or subahlo, the only difference among them is that for the halo or the subhalo, the mass of the SMBH depends differently on the mass of the halo. It is important to mention that in order to account for the substructure luminosity, an integration of the substructure mass function multiplied by the luminosity of an individual subhalo in all the substructure mass range must be performed. This integration should be done between m_{free}, the free streaming mass of the WIMP (the minimum mass that a virialized DM halo can have), and M_{main}, the mass of the main halo (no substructure can be as massive as the main halo). The free streaming mass will depend naturally on the WIMP mass, as $m_{free} \propto m_\chi^{-3}$. Based on the analysis of the effects of the free streaming length on the matter power spectrum by Angulo & White (2010), we consider a free streaming mass of $m_\chi = 10^{-10} M_\odot$ for a WIMP mass of $m_\chi = 1TeV$, and a free streaming mass of $m_\chi = 10^{-4} M_\odot$ for a WIMP mass of $m_\chi = 10GeV$.

We explicitly compute the luminosity of DM haloes, in the ΛCDM cosmology, considering two different WIMP masses (10GeV and 1TeV) and the presence or absence of substructure and adiabatic compression. We show the results obtained in Figure 3.

It can be seen that, for the same halo mass, the luminosity of the halo increases with redshift. This is a result of the structure formation process, because a DM halo that formed earlier will be more concentrated and have a higher characteristic density. Thus, its annihilation rate, and in consequence its luminosity, will be increased. Also, it can be seen that the greatest effect on the luminosity comes from the WIMP mass. In accordance with what was found for the smooth case, L_χ is almost inversely proportional to m_χ. There are variations to this proportionality, in the cases with substructure and adiabatic compression, because the maximum attainable mass of the compressed spike, as well as the minimum mass (free streaming mass) of the substructure are also dependent on m_χ. These deviations are, however, minimal. It can be also seen that the second greatest effect on the luminosity comes from the presence of adiabatic compression, and that the presence of substructure is the less important boosting mechanism.

It is also important to mention that according to Natarajan, Croton & Bertone (2008), the energy output required to offset the cooling flows in galaxy clusters (in order to quench star formation at low redshifts in galaxy cluster systems, and recover the properties of the Red Sequence), that in current semi-analytic models of galaxy formation is provided by AGN feedback, is on the order of $10^{35} - 10^{37} J/s$

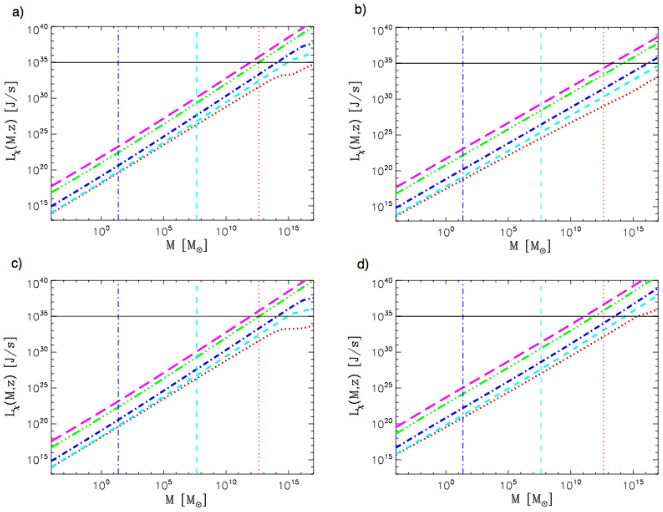

Figure 3. The internal DM annihilation luminosity of individual haloes, as a function of halo mass (in the range from 10^{-4} to 10^{17} $M_\odot$). The different curves in the four plots correspond to different redshifts; in particular, the dotted curves correspond to z = 0, the short-dashed curves correspond to z=3.6, the dot-dashed curves correspond to z = 10, the triple-dot-dashed curves to z = 50.1 and the long-dashed curves to z = 100. The different plots correspond to different clustering scenarios and WIMP masses; in particular, the top-left plot corresponds to the case with substructure and adiabatic compression, with a WIMP mass of 1TeV; the top-right plot corresponds to the case with substructure and 1TeV WIMP mass, but with no adiabatic compression; the bottom-left plot corresponds to the case with a WIMP mass of 1TeV and adiabatic compression, but no substructure; and the bottom-right plot corresponds to the case with adiabatic compression and substructure, but a WIMP mass of 10GeV. In all the plots we also include the $\nu = 1$ mass values for the 3 lowest redshifts in the corresponding line-styles, and the $10^{35} J/s$ luminosity threshold corresponding to AGN feedback in galaxy cluster-sized systems.

and thus, in general, the luminosities that we obtained are lower than the required value (by some $2-4$ orders of magnitude, except in the case of $m_\chi = 10GeV$, but this needs further study). It should be remembered that, although we plot halo luminosities up to haloes of mass of 10^{17}, the most massive gravitationally bound haloes today (at $z = 0$), have masses of the order of $10^{15} M_\odot$, so more massive haloes are virtually non-existent; and further more, the masses of the haloes that have a particular number density at a certain redshift (given by the characteristic dimensionless mass (ν)), falls rapidly with redshift. For clarity, we also include in Figure 3, the lines corresponding to $\nu = 1$ at different redshifts and the $10^{35} J/s$ luminosity threshold of AGN feedback in galaxy cluster-sized systems.

4.3 The global, clumped, DM annihilation luminosity per baryon

Having computed the DM annihilation luminosity of a particular halo of mass M at redshift z, we now return to the problem of computing the global energy injection rate to the IGM per baryon, but considering the clumpiness of the DM on all clustering scales. To do this, we simply consider that, knowing the luminosity of a particular halo (that already includes substructure and adiabatic compression), and knowing the halo mass function (calculated in Section 3.1), the energy output rate density (or luminosity density) due to DM annihilations is given simply by:

$$\epsilon_\chi^{clumped}(z) = (1+z)^3 \int_{m_{free}}^{m_{max}} L_\chi(M,z) \frac{dn}{dM}(M,z) dM, \quad (36)$$

where m_{free} is the free-streaming mass, m_{max} is the maximum mass of a DM halo, L_χ is the total DM annihilation luminosity (main halo plus substructure) of a DM halo of mass M at redshift z, $\frac{dn}{dM}$ is the previously calculated halo mass function (in comoving coordinates), and the factor $(1+z)^3$ is to convert the comoving density to a proper density. We consider $m_{max} = 10^{17} M_\odot$ since the number density of collapsed DM haloes with mass above this limiting mass is negligible.

Finally, the energy injection rate to the IGM per baryon can be directly computed as:

$$\dot{E}_\chi^{clumped}(z) = \frac{\epsilon_\chi^{clumped}(z)}{n_b(z)}, \quad (37)$$

where $n_b(z)$ is the proper number density of baryons at redshift z (equal to $(1+z)^3 n_{b,0}$ in terms of the present day baryon number density computed in Section 4.1).

It is important to mention that the energy injection rate to the IGM per baryon computed in this way, considers only the contribution of the DM haloes and not of the smooth component. In the case of a zero free-streaming mass, all the DM would be in haloes since there would be no minimum mass scale for the formation of collapsed structures. However, due to the non-zero free streaming mass, all haloes with masses less than that value, that should exist according to the halo mass function, are simply not allowed to form. As the clumped energy injection should be always greater than the smooth energy injection (computed in Section 4.1), and as the contribution due to DM haloes will be declining rapidly with increasing redshift after the truncation of low mass haloes due to the free-streaming limit becoming important, a good approximation is to use as the clumped DM injection rate the greater value among the one calculated in equation (47), and the one calculated in Section 4.1. This is the approach that was used for the case of a $10GeV$ WIMP.

The results obtained for the clumped energy injection rate per baryon, considering different clustering scenarios and WIMP masses, are shown in Figure 4. We only consider the maximal absorption fraction ($f_{abs} = 1$), because for other values, the resulting curves should simply be rescaled by f_{abs}.

It can be seen that the case considering a WIMP with mass of $10GeV$ is the one that gives the higher injection rate, in agreement with what was discussed above, for redshifts lower than a certain value of $z \sim 50$, and gives the lower injection rate for higher redshifts up to $z \sim 100$. This can be understood as a consequence of the higher free-streaming mass (and thus, higher minimum mass that haloes can have), and the fact that the mass of the haloes that have a characteristic $\nu = 1$ (the haloes that have just recently collapsed) decreases with increasing redshift, such that with a higher free-streaming mass, less haloes are allowed to form at higher redshifts. Also, the presence of adiabatic compression is important for boosting the energy injection rate, but only at

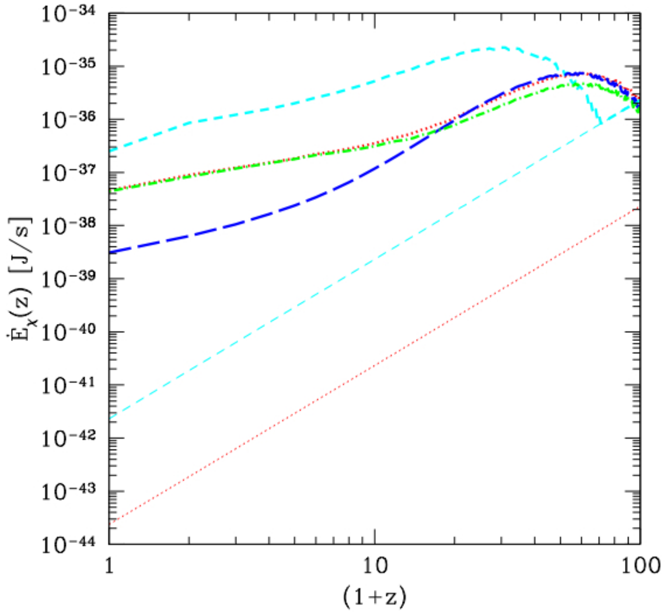

Figure 4. The clumped energy injection rate per baryon ($\dot{E}_\chi(z)$) as a function of redshift, for different scenarios, in thick lines. The dotted curve corresponds to the case with substructure and adiabatic compression for a WIMP mass of 1TeV, the long-dashed curve corresponds to the case with 1TeV WIMP mass and substructure but no adiabatic compression, the dot-dashed curve corresponds to the case of 1TeV WIMP with adiabatic compression but no substructure, and the short-dashed curve corresponds to a WIMP mass of 10GeV with substructure and adiabatic compression. Also included as thin lines are the previous curves of Figure 2, corresponding to the smooth cases, for a 1TeV WIMP (dotted) and a 10GeV WIMP (short-dashed).

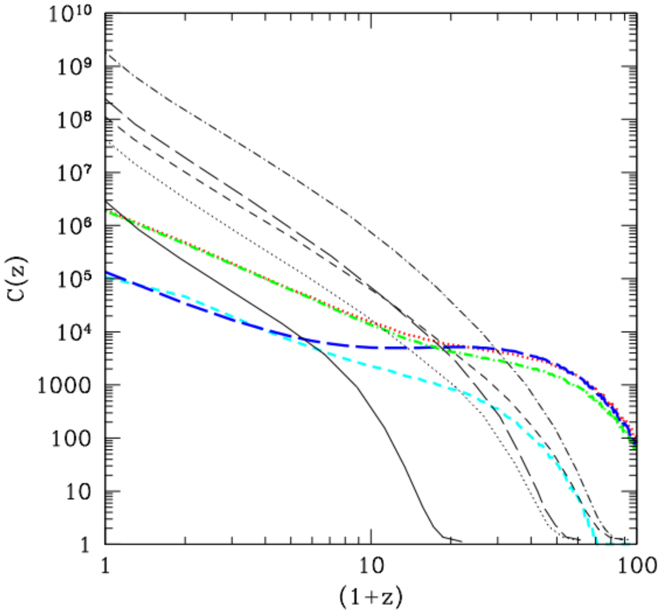

Figure 5. The clumpiness factor C(z) as a function of redshift. The thick curves correspond to our results. The line-styles of the thick curves are given as in Figure 4. For comparison, we also include the curves obtained by Cumberbatch, Lattanzi & Silk (2010) for the case of an NFW profile, taken from the upper panel of their Figure 3, as thin curves. The line-styles of the thin curves correspond to different values of (M_{min}/M_{odot},M_{cut}/M_{odot}). The solid line corresponds to (10^6,10^6), the dotted line corresponds to (10^{-4},10^6), the long-dashed line corresponds to (10^{-4},10^{-4}), the short-dashed line corresponds to (10^{-12},10^6) and the dot-dashed line corresponds to (10^{-12},10^{-12}). We refer the reader to the paper of the authors for further details.

redshifts lower than 10. The presence of substructure is the least important of the boost mechanisms.

In the next section, we obtain the clumpiness factor, C(z), implied by our energy injection calculations, and compare our results with those obtained by Cumberbatch, Lattanzi & Silk (2010).

4.4 The clumpiness factor

The clumpiness factor is a useful tool when accounting for DM clustering in global DM annihilation energy injection computations, like the ones required for calculating the heating and ionization of the IGM due to DM (see Section 6.1 and Section 6.2). It simply relates the clumped energy injection to the smooth one by:

$$C(z) = \frac{\dot{E}_\chi^{clumped}(z)}{\dot{E}_\chi^{smooth}(z)}. \tag{38}$$

We show the values obtained for the clumpiness factor C(z) in Figure 5. The meaning of the curves are explained in the caption.

In general, it can be seen that for all the cases considered, the clumpiness is a decreasing function of redshift. This is reasonable, because as the redshift increases, the universe will tend to be more homogeneous and uniform, because the gravitational collapse and formation of structures would have had less and less time to occur. Also, for all the cases considered, the universe will be practically completely homogeneous by redshift ($z \sim 150$), except for the case with $10GeV$ DM WIMP, in which the universe becomes homogeneous at redshift ($z \sim 70$). Note that in this case, although $\dot{E}_\chi^{clumped}(z)$ is higher than for the other cases by almost an order of magnitude at redshift zero, $\dot{E}_\chi^{smooth}(z)$ is higher as well, and so the clumpiness C(z) is not. It can also be seen that in agreement with what was discussed before, the adiabatic compression mechanism is important for low redshifts, and the presence of substructure is the less important mechanism for increasing the clumpiness.

We show also the clumpiness factors $C(z)$ obtained by Cumberbatch, Lattanzi & Silk (2010), in Figure 5, using different line-styles. The two sets of curves can be readily compared as the definitions of the clumpiness factors are the same. There are, however, differences in the methods for computing them. In particular, Cumberbatch, Lattanzi & Silk (2010) compute the halo mass function using the P-S theory, starting from an analytic fit to $\sigma(M, z)$, and then consider that substructure and sub-substructure follow a pure power-law mass function with exponent -2. We refer the reader to the authors for further detail about their computation procedure. In general, it can be seen that we predict less clumpiness than the authors at low redshift, but higher clumpiness than the authors at high redshift. This can be understood because the authors also include sub-substructure (sub-subhaloes within subhaloes), that may be more important near redshift zero, but we include adiabatic compression (and they do not), which may be important at higher redshifts than substructure, but low enough so that formation of haloes is not disfavoured by the free-streaming mass.

Having computed the energy output due to DM annihilations of local haloes, and having obtained the energy injection rate into the IGM per baryon in the perfectly smooth case and in the clumped case, considering a standard thermal relic WIMP cross section, we consider in the next section the Sommerfeld enhancement, a physical process that may be responsible for enhancing the annihilation cross section by as much as 3 orders of magnitude.

We do not include Sommerfeld enhancement in our calculations, because it is highly dependent on unknown physics (the mass of the new force carrier and the resulting potential, as well as the physical scenarios in which this new force could arise), however, its effect is to directly modify $< \sigma v >$ by a constant factor. As we already mentioned in the Introduction, the presence of Sommerfeld enhancement is controversial and not supported by all observational evidence.

Having computed the DM annihilation luminosity generated within a DM halo for different scenarios, in the next section we study the luminosity received by a DM halo due to the rest of the universe.

5 EXTERNAL DM ANNIHILATION ENERGY INJECTION ON A HALO

On previous sections, we have considered particular WIMP models, calculated the DM clustering on all scales explicitly, and computed the DM annihilation luminosity generated within a particular DM halo, and the energy injection per baryon on the IGM. In this section, we calculate the DM annihilation luminosity received by a halo due to the energy generated in the rest of the universe. For this, we will use the formalism developed so far, and calculate the energy output of a distant halo that is received by a particular halo. Also, we will use the bias factor and the two-point correlation function, that allow to calculate the spatial clustering statistics of haloes around a particular halo. Then, combining these, we will calculate the desired energy received by the halo from all DM structures external to it.

In the next subsection, we consider and compute the luminosity that is received by a distant halo.

5.1 The luminosity received by a distant halo

The flux received by an astronomical source, located at a nearby distance d, follows the usual relation:

$$f = \frac{L}{4\pi d^2}. \tag{39}$$

In the case of cosmological distances, the distance d should be replaced by the luminosity distance $d_L(r)$, that is a function of the comoving distance r to the source (equal to the proper distance at redshift zero). Also, if one wants to compute the received luminosity (energy per unit time) from the source, one should multiply the flux f by the cross section to photons of the surface that receives the radiation (e.g., πR^2 for a sphere). Finally, if the travelling photon has a non-zero probability of being absorbed in the way, and thus may not arrive at the receiving surface, this should be accounted for by the addition of a certain transfer function. Thus, the desired luminosity that is received by a distant halo can be written as:

$$L_{\chi,i}(M, M_i, z, r) = \frac{L_\chi(M_i, z_i(z,r)) f_T(r) \sigma_{bary}(M)}{4\pi d_L^2(z,r)}, \tag{40}$$

where $L_{\chi,i}(M, M_i, z, r)$ corresponds to the luminosity that is received by a halo of mass M at redshift z, due to a halo i of mass M_i located at a comoving distance r from the first halo. The function $f_T(r)$ corresponds to the transmittance function, $\sigma_{bary}(M)$ corresponds to the baryonic cross-section of the receiving halo, $z_i(z,r)$ corresponds to the redshift at which a photon is emitted by halo i such that it arrives to the receiving halo at redshift z, and $d_L(z,r)$ is the luminosity distance between two halos separated by a comoving distance r at redshift z.

For obtaining the redshift of emission ($z_i(z,r)$), we consider that the comoving distance travelled by a photon emitted at redshift z_2 and received at z_1 is given by:

$$r = \int_{\frac{1}{1+z_2}}^{\frac{1}{1+z_1}} \frac{c\,da}{a^2 H(a)}. \tag{41}$$

This gives $z_i = z_i(z,r)$ as an implicit function that can be evaluated numerically.

For computing the luminosity distance between two objects separated by a comoving distance of r at redshift z (not to be confused with the luminosity distance of an object at redshift z with respect to an observer at redshift zero), we use

$$d_L(r,z) = \left(\frac{1}{1+z}\right) S_k(r) \frac{(1+z_i(z,r))}{1+z}, \tag{42}$$

where the function $S_k(r)$ corresponds to the cosmological distance measure (given by the angular part of the Robertson-Walker metric), and is different for flat and curved cosmologies. For a flat case (Einstein-De Sitter and ΛCDM cosmologies), $S_k(r) = r$.

For the halo cross section, we consider a baryonic cross section given by:

$$\sigma_{bary}(M) = (r_{bary,MW})^2 \pi \frac{M^{2/3}}{M_{MW,halo}^{2/3}}, \tag{43}$$

where $r_{bary,MW} = 0.01 Mpc$ and $M_{MW,halo} = 10^{12} M_\odot$ are fiducial values for the baryonic radius and halo mass of a MW-like DM halo. We therefore consider that the cross section of photon absorption of a halo scales as its mass to the 2/3 power, or in other words, as its transversal area. We also consider that the baryons are responsible for the photon absorption, that the cross section is redshift-independent, and that it does not depend on halo orientation. This cross section is in proper Mpc^2.

The transmittance function was obtained by analogy to radiative transfer theory. If the cross section of a DM halo depends only on its mass, we can define an optical depth for DM-annihilation-generated photons travelling through the universe as:

$$\tau(z) = \int_{m_{free}}^{m_{max}} \sigma(M) \frac{dn}{dM} (1+z)^2 dM, \tag{44}$$

where the $(1+z)^2$ factor is to convert the cross section to comoving coordinates.

Then, the transmittance function is simply given in terms of the optical depth by:

$$f_T(r,z) = e^{-\tau(z)\epsilon_{abs} r}, \tag{45}$$

where ϵ_{abs} is the fraction of photons that are indeed absorbed when they pass through the cross-section of a halo.

Now, all the functions used in the computation of $L_{\chi,i}$ (the luminosity received due to halo i) have been specified. In the next section, we explain the two-point correlation function that measures the spatial clustering of haloes.

5.2 The two-point correlation function

The correlation functions we will consider take into account redshift evolution

Although the correlation function is completely specified by the power spectrum, the $P(k)$ that we calculated is valid in the linear theory approximation, and thus, it is not a good estimator of the DM halo spatial clustering on small scales. Therefore, we will use a standard analytic fit to the zero redshift correlation function, as a pure power law, with its exponent and normalization motivated by observation (for example the Sloan Digital Sky Survey, as analysed by Zehavi et al. (2011)) and simulations:

$$\xi_0(r) = \left(\frac{r}{6h^{-1}Mpc} \right)^{-1.8}, \tag{46}$$

where r is in comoving Mpc.

In the next section we explain the bias factor, that represents the excess in clustering of haloes above different mass scales.

5.3 The bias factor

In the previous section, we defined the correlation function $\xi(r,z)$ as the excess clustering of the matter density field on characteristic separations r at redshift z. DM haloes with different masses (above a mass scale M), provide biased measurements of clustering. The bias factor of mass scale M can be defined by:

$$b^2(M,z) = \frac{\xi_{MM}(r,z)}{\xi_{DM}(r,z)}, \tag{47}$$

with $\xi_{MM}(r,z)$ the correlation function of the DM haloes with masses above M, and $\xi_{DM}(r,z)$ the unbiased correlation function (labelled simply as $\xi(r,z)$, and considered previously). This bias factor is independent of r in a first order approx.

We adopt the bias factor given by Sheth, Mo & Tormen (2001) that takes into account ellipsoidal collapse and fits well numerical simulation measurements.

5.4 The external luminosity received by a halo

We now have all the pieces required to compute the external luminosity received by a DM halo due to all DM haloes external to it. First, we consider the radial halo mass function, that will be given by the mass function computed with P-S theory, but considering the clustering of DM around the particular halo of mass M:

$$\frac{dn}{dM_i}(M, M_i, z, r) = (1 + b(\nu(M_i,z))b(\nu(M,z)) \times \\ \times \xi(r,z)) \frac{dn}{dM_i}(M_i, z). \tag{48}$$

Now we define the radial emissivity, as the DM annihilation energy generation rate per comoving volume at a distance r from the halo of mass M:

$$\epsilon_\chi(M,z,r) = \int_{m_{free}}^{m_{max}} \frac{dn}{dM_i}(M, M_i, z, r) \times \\ \times L_{\chi,i}(M, M_i, z, r) dM_i. \tag{49}$$

Finally, the required external luminosity will be given by:

$$L_\chi^{ext}(M,z) = \epsilon_{abs}\epsilon_{esc} \int_{r_{vir}(M,z)}^{r_{max}} 4\pi S_k^2(r) \epsilon_\chi(M,z,r) dr. \tag{50}$$

The volume integration is performed between the comoving virial radius of the halo up to r_{max}. Formally, r_{max} should be ∞ in the Open and Flat cosmologies, and πR_0 in closed cosmologies. However, in practice, we use a radius of $r_{max} = 1Gpc$, because at such large distances, the luminosity of individual haloes arrives so diluted that the contribution to the integral is negligible. We also consider the absorption and escape fractions ϵ_{abs} and ϵ_{esc}. This absorption and escape fractions are different to the previously discussed $f_{abs}(z)$, because they are the fraction of the DM annihilation energy that is trapped (absorbed) within haloes (ϵ_{abs}), and the fraction of the DM annihilation energy that manages to escape from haloes as photons and is free to propagate through the universe. We assume that $\epsilon_{abs} + \epsilon_{esc} = 1$, so that no energy is wasted, and consider $\epsilon_{abs} = 0.9$ and $\epsilon_{esc} = 0.1$. We choose these values because an escape fraction of 0.1 means that 10% of the photons manage to reach the IGM, and therefore, this choice is somewhat similar to choosing $f_{abs}(z) = 0.1$ as motivated by Cumberbatch, Lattanzi & Silk (2010) and Natarajan & Schwarz (2009), although both fractions are not directly comparable.

In Figure 6, we show our results for the external DM annihilation luminosity as a function of halo mass at different redshifts, considering only the ΛCDM cosmology, in the case of a WIMP with mass $1TeV$ and considering both substructure and adiabatic compression.

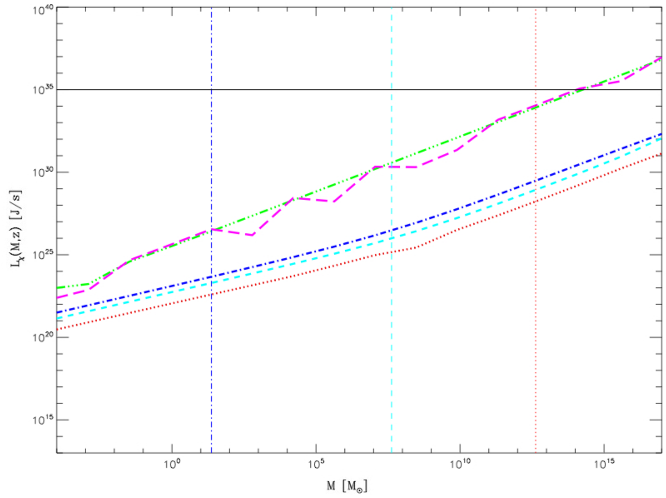

Figure 6. The external DM annihilation luminosity received by individual haloes, as a function of halo mass (in the range from 10^{-4} to 10^{17} $M_\odot$). The colours of the curves correspond to different redshifts; in particular, the dotted curve correspond to redshift zero, the short-dashed curve correspond to redshift 3.6, the dot-dashed curve correspond to redshift 10, the triple-dot-dashed curve to redshift 50.2 and the long-dashed curve to redshift 100. The curves were computed assuming a WIMP mass of 1TeV and considering both substructure and adiabatic compression. We also include the $\nu = 1$ mass values for the 3 lowest redshifts in the corresponding line-styles, and the $10^{35} J/s$ luminosity threshold corresponding to AGN feedback in galaxy cluster-sized systems, as in Figure 3.

In general, comparing these results with the ones obtained for the DM luminosity generated within a particular halo (see Figure 3), one can see that the external luminosity relation is less steep than the internal one, and so, therefore, the external luminosity will be more important than the internal luminosity for haloes below a certain mass ($\sim 10^3 - 10^4 M_\odot$), and less important for haloes above that mass. The implications of this have not yet been studied, but it will be interesting to do so as future work.

6 GLOBAL IGM HEATING, IONIZATION AND 21 CM SIGNAL DUE TO DM

Different authors have studied the effects of DM annihilations (or decays) on the global properties of the IGM, due to their extra energy injection (for example, see Pierpaoli (2004); Mapelli, Ferrara & Pierpaoli (2006); Ripamonti, Mapelli & Ferrara (2007); Valdés et al. (2007); Natarajan & Schwarz (2009); and Cumberbatch, Lattanzi & Silk (2010) among others). In this section, we study the effects on the IGM of the energy injection found on Section 4.3. We divide the section into different subsections, each corresponding to one of the different physical quantities of interest that are affected by this extra energy injection. We explain the formalism and the definition of the quantities, as well as how to compute them, in the beginning of the corresponding subsections, and then we show the results we obtained and compare them with different authors. The first two sections (the ionization fraction and the IGM temperature), refer to general properties of the IGM, whereas the next sections have to do with the signal of this extra-heating on the 21 cm line of the hyperfine structure of neutral hydrogen (HI).

We start, in the next subsection, with the computation of the IGM ionization fraction.

6.1 The IGM ionization fraction

The ionization fraction (x_e) is defined as the ratio of free electrons to hydrogen atoms $x_e = \frac{n_e}{n_H}$. Following Valdés et al. (2007), the variation of the ionization fraction is given by:

$$\frac{dx_e}{dz} = \frac{1}{H(z)(1+z)} \left[R_s(z) - I_s(z) - I_\chi(z) \right], \qquad (51)$$

where I_s and R_s are the standard ionization and recombination rates per baryon, and $I_\chi = \chi_i(z) \frac{\dot{E}_\chi}{E_0}$ is the contribution to the ionization rate due to the energy injection of DM annihilation. $\dot{E}_\chi$ is the energy injection rate per baryon computed in Section 4.3, E_0 is the ionization energy of Hydrogen (13.6 eV), and $\chi_i(z)$ is the ionization efficiency and is given by $\chi_i(z) = \frac{1-x_e}{3}$ (i.e., if all matter is ionized, no energy is used for ionization, and if all matter is neutral, 1/3 of the injected energy goes to ionizations). The factor $\frac{1}{H(z)(1+z)}$, is simply a change of variables, because the differential of cosmic time dt and the redshift differential dz are related by $dt = \frac{-dz}{H(z)(1+z)}$.

We define the DM annihilation contribution to the ionization fraction as $\delta x_e(z) = x_e(z) - x_e^{no-DM}(z)$, where x_e^{no-DM} is the ionization fraction in the standard scenario. It is important to mention that this standard ionization fraction is a consequence of the physics of recombination from the epoch of the last scattering surface, and is simply the relic free-electron abundance from the freeze-out of the recombination reaction. Thus, the x_e^{no-DM} does not account for the reionization of the universe by Poulation III stars, that according to WMAP7 (Komatsu et al. 2011), occurred at redshift 10.6 ± 1.2. With this definition of δx_e, we have:

$$\frac{d\delta x_e}{dz} = \frac{-I_\chi(z)}{H(z)(1+z)}. \qquad (52)$$

We solve this differential equation, using the x_e^{no-DM} given in Figure 3 of Mapelli, Ferrara & Pierpaoli (2006), by the Euler method, using as boundary condition that $\delta x_e(z = 1000) = 0$ (at redshift $z > 1000$, as we are near the recombination epoch, the ionization fraction is near 1 and is almost entirely due to the standard cooling scenario).

We show the obtained ionization fraction ($x_e(z)$) curves in Figure 7 and in Figure 8. The first figure shows the $x_e(z)$ curves obtained for the different DM clustering scenarios and WIMP masses, but considering the clumped DM case, and with an absorption fraction of $f_{abs} = 1$ (more details on the caption of the figure). The second figure shows the ionization fractions, assuming a WIMP mass of 1TeV and substructure and adiabatic compression, but for different values of the absorption fraction ($f_{abs} = 0.1$ or 0.01), or simply not considering DM clustering at all, and using the homogeneous DM energy injection computed previously.

It can be seen from Figure 7 that the ionization fraction evolves very differently from the case with no DM energy in-

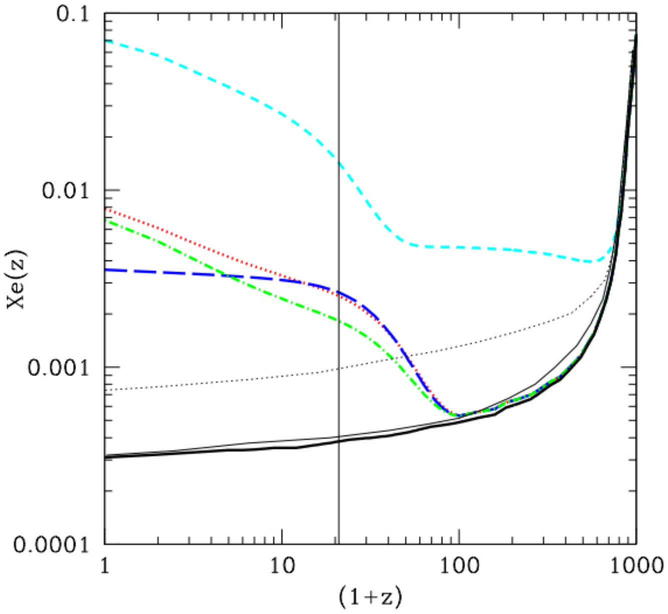

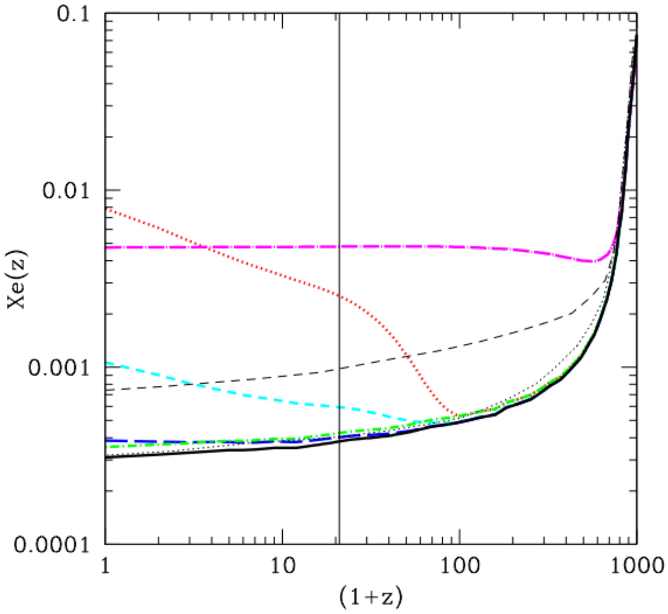

Figure 7. The ionization fraction of the IGM for different cases, assuming a maximal absorption fraction and the clumpiness of the DM. Our results are shown as thick lines. The different line-styles of the thick lines correspond to: (short-dashed) a WIMP mass of 10GeV with adiabatic compression and substructure, (dotted) a WIMP mass of 1TeV with adiabatic compression and substructure, (long-dashed) a WIMP mass of 1TeV with substructure but no adiabatic compression, (dot-dashed) a WIMP mass of 1TeV with adiabatic compression but no substructure, and (solid) the standard cooling scenario, with no DM energy injection. For comparison, we also include the results obtained by Mapelli, Ferrara & Pierpaoli (2006) for the case of the 100GeV SUSY neutralino, taken from the bottom panel of Figure 3 of the authors and we show them as thin lines. The thin solid line corresponds to $<\sigma v>= 2\times10^{-26}cm^3s^{-1}$ and the thin dotted line corresponds to $<\sigma v>= 10^{-24}cm^3s^{-1}$. Also included is the line corresponding to $z = 20$, that indicates when the effects of Population III stars may become important.

Figure 8. The ionization fraction of the IGM for different cases, assuming a WIMP mass of 1TeV and substructure and clustering, or no DM clumpiness at all. Our results are shown as thick lines. The different line-styles of the thick lines correspond to: (dotted) the standard clustering scenario considering both substructure and adiabatic compression with a 1TeV WIMP and $f_{abs} = 1$, (short-dashed) the same clustering scenario but considering $f_{abs} = 0.1$, (long-dashed) the same clustering scenario but with $f_{abs} = 0.01$, (short-dot-dashed) the same WIMP mass but considering no DM clumpiness, (long-dot-dashed) a 10GeV WIMP with no DM clumpiness, and (solid) the standard cooling scenario, with no DM energy injection. For comparison, we also include the results obtained by Mapelli, Ferrara & Pierpaoli (2006) for the case of the 100GeV SUSY neutralino, taken from the bottom panel of Figure 3 of the authors and we show them as thin lines. The thin solid line corresponds to $<\sigma v>= 2\times10^{-26}cm^3s^{-1}$ and the thin dotted line corresponds to $<\sigma v>= 10^{-24}cm^3s^{-1}$. Also included is the line corresponding to $z = 20$, that indicates when the effects of Population III stars may become important.

jection, as long as the DM clumpiness is considered. Also, for the case of a WIMP with a mass of $10GeV$, the ionization fraction can be increased up to $x_e \sim 0.1$ at redshift zero, whereas for the other cases that consider a 1TeV WIMP, this partial re-ionization can only bring x_e to ~ 0.01 at redshift zero, hence leading to a difference of one order of magnitude of the final ionization fraction (note, however, that as the computation of the ionization fraction does not account for the Population III stars, that are thought to have re-ionized the universe at redshift $z \sim 10$, this results are only reliable down to that redshift at most; however we use a more conservative limit of $z = 20$ in the plots, to account for the fact that the formation of the first stars started earlier than the actual redshift of reionization). It can also be seen that both substructure and adiabatic compression are considerably less important in determining the evolution of the ionization fraction, and that adiabatic compression is more relevant near redshift zero, whereas substructure is more important between redshifts $\sim 7- \sim 100$.

From Figure 8, it can be seen that even without considering DM clumpiness, the case with a $10GeV$ WIMP considerably modifies the ionization fraction of the universe. It has the effect of raising the relic ionization at redshift 0 (without accounting for stellar populations) by a factor of ~ 20. Also, the evolution of the ionization fraction is particularly sensitive to the absorption fraction f_{abs}, such that reducing f_{abs} from 1 to 0.1 results in a completely different evolution (and in a ionization fraction at z=0 an order of magnitude lower). The cases with $f_{abs} = 0.1$ and no clumpiness give evolutions of the ionization fraction that are very similar to the case were no DM energy injection is present.

6.2 The IGM kinetic temperature

We now consider the kinetic temperature of the IGM. Following Valdés et al. (2007), the change in this temperature is given by:

$$(1+z)\frac{dT_k}{dz} = 2T_k + \frac{l_\gamma x_e}{H(z)(1+Y+x_e)}(T_k - T_{CMB}) -$$

$$-\frac{2\chi_h \dot{E}_\chi}{3k_b H(z)(1+Y+x_e)}, \qquad (53)$$

where $l_\gamma = \frac{(8\sigma_T a_R T^4_{CMB})}{(3m_e c)}$ is the analogue to a thermal conductivity between the CMB and the IGM, χ_h is the heating efficiency and is given by $\chi_h = \frac{1+2x_e}{3}$ and Y is the helium fraction by mass (taken as $Y = 0.26$).

It is expected (see for example Cumberbatch, Lattanzi & Silk (2010)) that the IGM kinetic temperature tracks the CMB temperature at high redshifts, so we used the CMB temperature at redshift $z = 1000$ as the boundary condition for the IGM kinetic temperature, and solved the differential equation by the Euler method. The interpretation of this cooling equation is straightforward, as the first term on the right hand side corresponds to the adiabatic cooling of the IGM in absence of heat exchange or energy injection, and proceeds as $T \propto (1+z)^2$. The second term corresponds to the heat exchange between the CMB and the IGM, and the third term allows for the extra heating due to the DM annihilation energy injection.

We show the obtained IGM kinetic temperature curves in Figure 9 and in Figure 10. The first figure shows the temperatures obtained for the different DM clustering scenarios and WIMP masses, but considering the clumped DM case, and with an absorption fraction of $f_{abs} = 1$ (more details on the caption of the figure). The second figure shows the temperatures, assuming a WIMP mass of 1TeV and substructure and adiabatic compression, but for different values of the absorption fraction ($f_{abs} = 0.1$ or 0.01), or simply not considering DM clustering at all, and using the homogeneous DM energy injection computed previously.

In can be seen on Figure 9 that for all the cases that consider the clumpiness of the DM (assuming $f_{abs} = 1$), the cooling is very different from the standard adiabatic scenario. Significant re-heating occurs in the case of a $10GeV$ WIMP, where the IGM may be heated even to temperatures of $1000K$ by redshift zero (although, remember that this cooling scenario does not account for energy injection due to stellar components and so it is reliable only down to redshift $z \sim 20$). Also, adiabatic compression is more important for the cooling history than substructure, and the extra heating due to this compression can amount to an order of magnitude of difference by redshift zero.

Also, it can be seen on Figure 10 that the absorption fraction is critical for determining the particular cooling history, and that the low-redshift heating due to DM annihilations can vary enormously with different choices for f_{abs}. It can be seen that, in general, in the cases considering adiabatic compression, the IGM kinetic temperature reaches a quasi-stationary state, and the final temperature attained is almost proportional to the absorption fraction.

We also include the results for the ionization fraction and IGM kinetic temperature obtained by Mapelli, Ferrara & Pierpaoli (2006), in order to compare them with our results.

It can be seen that for the cases with no DM clumpiness, we reproduce the results obtained by the authors. Also, the boost they considered in the cross section (for example, accounting for Sommerfeld enhancement), has almost exactly the same effect than lowering the mass of the WIMP particle. Furthermore, we find significant effects not accounted for by the authors when considering the clumpiness of the DM on all its levels.

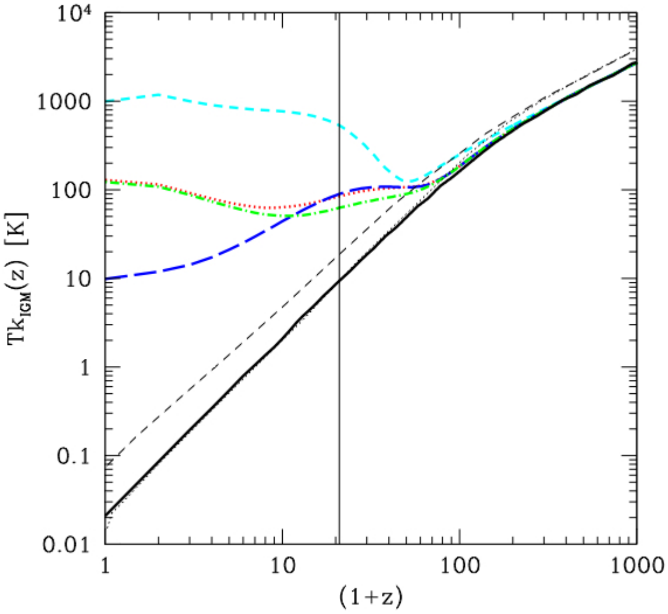

Figure 9. The kinetic temperature of the IGM for different cases, assuming a maximal absorption fraction and the clumpiness of the DM. For comparison, we also include the results of Mapelli, Ferrara & Pierpaoli (2006), taken from the top panel of Figure 3 of the authors. The different line-styles are assigned in the same way as in Figure 7. The $z = 20$ line is also included.

6.3 The neutral hydrogen spin temperature

We now study the 21 cm signal from neutral hydrogen, and how it is modified by DM annihilation. We follow Cumberbatch, Lattanzi & Silk (2010) and Valdés et al. (2007) in the explanation of the physics and the processes involved, and refer the reader to the above papers for further details.

The 21 cm line corresponds to the transition energy between the singlet and triplet hyperfine levels ($n = 0$, $j = 0$ and $n = 0$, $j = 1$) of the hydrogen atom. The spin temperature of the neutral hydrogen is defined as the temperature that relates the populations of singlet and triplet states:

$$\frac{n_1}{n_0} = 3e^{-\frac{T_*}{T_s}}, \qquad (54)$$

where T_s is the spin temperature, T_* is the equivalent temperature of the 21 cm transition (corresponding to $T_* = \frac{hc}{\lambda k_B}$, where $\lambda = 21cm$), n_1 is the triplet state occupation number, n_0 is the singlet state occupation number and the factor of 3 is the degeneracy of the triplet state (i.e., 3).

In general, the spin temperature is a weighted average of the IGM kinetic temperature and the CMB temperature. In absence of additional heating mechanisms, both the IGM

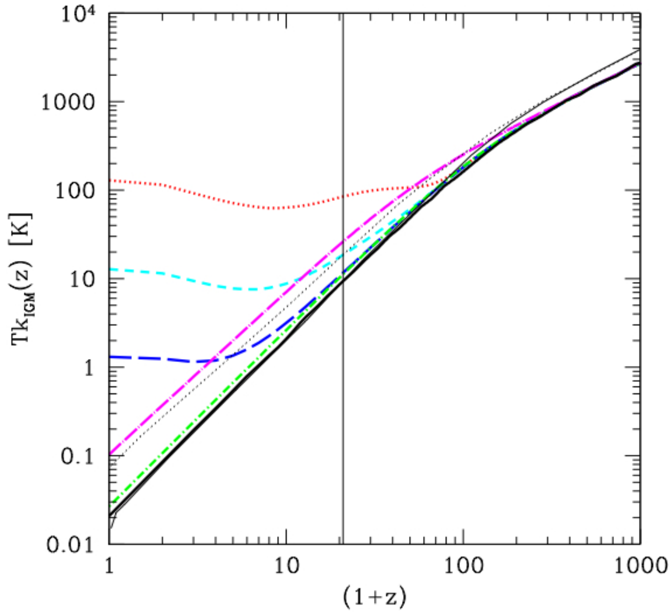

Figure 10. The kinetic temperature of the IGM for different cases, assuming a WIMP mass of 1TeV and substructure and clustering, or no DM clumpiness at all. For comparison, we also include the results of Mapelli, Ferrara & Pierpaoli (2006), taken from the top panel of Figure 3 of the authors. The different line-styles are assigned in the same way as in Figure 8. The $z = 20$ line is also included.

kinetic temperature and the spin temperature are coupled to the CMB at high redshifts ($z \gtrsim 300$), whereas at lower redshifts, the IGM cools faster than the CMB. Thus, the spin temperature will be lower than the CMB and the IGM will be visible in 21 cm absorption.

There are two main mechanisms that couple the spin temperature and the kinetic temperature: Spin exchange collisions and Ly-alpha pumping (also called the Wouthuysen-Field (W-F) effect (Hirata 2006)). Spin exchange collisions correspond to the collisions of neutral hydrogen (responsible for the 21 cm line) with other neutral hydrogen atoms, with electrons or with protons. These collisions will tend to thermalize the populations of both levels (singlet and triplet) to the kinetic temperature of the IGM, and thus will couple T_s with T_k. Lyman-alpha pumping, on the other hand, corresponds to the mixing (and thus thermalisation) of the singlet and triplet levels by Lyman-alpha transitions (from energy levels 1 to 2 and vice-versa) to the 2p level. Therefore, the mixing of hyperfine states through the W-F effect will depend on the intensity of the Lyman-alpha photon field, which in turn will depend on the kinetic temperature of the IGM and on the direct energy injection due to DM WIMPS. Thus, the W-F will also couple T_s with T_k.

At low redshift ($z < 50$), the IGM density is sufficiently rarefied so as to make the spin exchange collisions too improbable, and thus T_s will tend to follow the temperature of the CMB again.

As the mechanisms coupling T_s and Tk_{IGM} depend on the ionization fraction x_e, and the DM energy injection rate per baryon $\dot{E}_\chi$, it is expected that the presence of an annihilating WIMP will alter the evolution of T_s with redshift, and thus, the detection of this signal may help to discriminate between different WIMP scenarios.

The spin temperature at redshift z can be computed as:

$$T_s = \frac{T_{CMB} + y_\alpha T_k + y_c T_k}{1 + y_\alpha + y_c}, \qquad (55)$$

where y_α is the W-F coupling, and y_c is the collisional coupling to the IGM temperature. The coupling coefficients can be computed as:

$$y_\alpha = \frac{P_{10} T_*}{A_{10} T_k}, \qquad (56)$$

and

$$y_c = \frac{C_{10} T_*}{A_{10} T_k}, \qquad (57)$$

where $A_{10} = 2.85 \times 10^{-15} s^{-1}$ is the spontaneous emission coefficient for the transition, and P_{10} and C_{10} are the radiative and collisional transition coefficients respectively (they are rates, with units of $\left[s^{-1}\right]$). The collisional transition coefficient is given by:

$$C_{10} = k_{10} n_{HI} + n_e \gamma_e, \qquad (58)$$

where n_{HI} and n_e are the neutral hydrogen number density and the free electron number density respectively, and k_{10} and γ_e are the specific (one particle) transition coefficients for collisions with neutral hydrogen atoms and electrons respectively. We have neglected the contribution due to collisions with protons, following Cumberbatch, Lattanzi & Silk (2010). The number densities n_e and n_{HI} are easily obtained in terms of the above-defined ionization fraction x_e, the hydrogen and helium abundances by number (f_H and f_{He}) and the baryonic density of the universe n_b, also defined previously. We use the following formulas for the coefficients k_{10} and γ_e:

$$k_{10} = 3.1 \times 10^{-11} T_k^{0.357} exp(-32K/T_k), \left[cm^3 s^{-1}\right]; \qquad (59)$$

and

$$log(\gamma_e/cm^3 s^{-1}) =$$

$$= -9.607 + 0.5 log(T_k/1K) exp(-[log(T_k/1K)]^{4.5}/1800),$$

$$1K < T_k < 10^4 K, \qquad (60)$$

$$log(\gamma_e/cm^3 s^{-1}) = -9.607 + 0.5 log(T_k/1K), T_k < 1K, \qquad (61)$$

$$\gamma_e(T_k > 10^4 K) = \gamma_e(10^4 K). \qquad (62)$$

The fit to k_{10} is given by Kuhlen, Madau & Montgomery (2006) and the fit to γ_e is given by Liszt (2001).

We now calculate P_{10} as:

$$P_{10} = \frac{16}{27}\frac{\pi J_\alpha \sigma_\alpha}{h\nu_\alpha}, \tag{63}$$

where J_α is the isotropic specific intensity of the radiation field in the Ly-alpha line, σ_α is the Ly-alpha transition cross-section in the monochromatic approximation, and ν_α is the frequency of the Ly-alpha transition photon. According to Laor (1996), the σ_α monochromatic cross-section is given by:

$$\sigma_\alpha = \frac{\pi e^2}{m_e c} f_{12} f_{se} \frac{n_1}{n_1 + n_2}, \tag{64}$$

where f_{se} is the stimulated emission correction and is given by:

$$f_{se} = (1 - e^{-\frac{h\nu_\alpha}{k_B T_k}}), \tag{65}$$

the first and second energy levels population ratio $\frac{n_2}{n_1}$ of the hydrogen atom is given by:

$$\frac{n_2}{n_1} = \frac{g_2}{g_1} e^{-\frac{h\nu_\alpha}{k_B T_k}}, \tag{66}$$

the $n - th$ level degeneration is given by $g_n = 2n^2$, and f_{12} is the oscillator strength of the transition ($f_{12} = 0.416$). Note that and the factor e^2 in σ_α should be replaced by $\frac{e^2}{4\pi\epsilon_0}$ when using MKS units.

Finally, the specific intensity of the Ly-alpha radiation field is given by:

$$J_\alpha(z) = \frac{n_H^2 hc}{4\pi H(z)} \left[x_e x_p \alpha^{eff}_{2^2P} + x_e x_{HI} \gamma_{eH} + \frac{\chi_\alpha \dot{E}_\chi(z)}{n_H h\nu_\alpha} \right], \tag{67}$$

where $x_p = (1 - x_{HI})$ is the proton fraction with respect to the total hydrogen number density, $\alpha^{eff}_{2^2P}$ is the radiative recombination coefficient to the $n = 2$, $l = 1$ level, given in Table 1 of Pengelly (1964), γ_{eH} is a collisional excitation rate of HI atoms involving electrons, and $\chi_\alpha = \frac{\chi_e}{2}$, where χ_e is the excitations efficiency given by $\chi_e = \frac{1-x_e}{3}$ (here, it can be seen that $\chi_e + \chi_i + \chi_h = 1$, and thus, all the energy injected to the IGM by DM annihilation goes to either heating, ionization or excitation). For γ_{eH}, we use:

$$\gamma_{eH} = 2.2 \times 10^{-8} exp\left[-11.84/(T/10^4 K)\right], [cm^3 s^{-1}], \tag{68}$$

given by Cumberbatch, Lattanzi & Silk (2010).

Now, we can explicitly compute the spin temperature T_s as a function of z, and use it in the following calculations.

6.4 The 21 cm differential brightness temperature

Having obtained the spin temperature T_s, we proceed to compute the 21 cm differential brightness temperature δT_b, defined as:

$$\delta T_b = \frac{T_s - T_{CMB}}{1 + z} \tau(z), \tag{69}$$

where τ is the optical depth of the neutral IGM at 21(1+z) cm, and can be calculated as:

$$\tau(z) = \frac{3c^3 h A_{10}}{32\pi k_B \nu_0^2 T_s(z) H(z)} n_{HI}(z), \tag{70}$$

where $\nu_0 = 1420 MHz$ is the frequency corresponding to the 21 cm transition in the rest frame of the source. The differential brightness temperature is important because it gives a difference in brightness between the CMB and the neutral hydrogen averaged in the beam of the instrument, and will be given by the above formula when the beam is large enough that the signal equals the average global one. Thus, this is the quantity that can be measured observationally in the low frequency range, and will be used for the next section.

6.5 The difference of differential brightness temperatures

Finally, we compute the difference in differential brightness temperature, defined as:

$$\Delta\delta T_b(z) = |\delta T_b(z) - \delta T_{b,0}(z)|, \tag{71}$$

where $\delta T_{b,0}(z)$ corresponds to the differential brightness temperature obtained without the extra energy injection by DM annihilations. According to Valdés et al. (2007), this signal could be measured with current and future radio telescopes, such as LOFAR, 21CMA, MWA and SKA, in principle, up to the $\approx 1mK$ level at redshifts where baryonic energy injection processes (such as Population III star formation) are not important ($z >\sim 20 - 30$). However, the authors explain that the various foregrounds (i.e., Galactic free-free and synchrotron emission, unresolved extragalactic radio sources, free-free emission from ionizing sources, synchrotron emission from cluster radio haloes and relics) are much stronger than the cosmological signal, and are also very difficult to remove. The authors also explain some possible methods for effectively removing the foregrounds and for clearly identifying the extra energy injection signal; however, that is beyond the scope of this work and we refer the reader to their paper.

In Figure 11 and in Figure 12, we show the results we obtained for the $\Delta\delta T_b(z)$ curve, for the different cases we considered. In Figure 11 we assume the maximal absorption fraction $f_{abs} = 1$, and consider the different DM clustering scenarios and WIMP masses. In Figure 12, we consider the standard scenario for the DM clustering (adiabatic compression with substructure), and we vary the absorption fraction, the WIMP mass, or consider the perfectly smooth case (for more details about the plots, see their captions).

It can be seen, from Figure 11, that the most important factor that determines the $\Delta\delta T_b$ signal is the WIMP mass. For a $10GeV$ WIMP, the signal is around $\sim 40[mK]$ at redshift 100, very much above the $\sim 1mK$ sensitivity of current and future instruments quoted by Valdés et al. (2007). However, the authors also mention that current and future radio frequency arrays will probe up to a minimum frequency of $30MHz$, thus corresponding to a 21cm emission at $z \sim 46$. Therefore, the sensitivity window should be considered as $\Delta\delta T_b > 1mK$, and also $\sim 20 < z <\sim 46$. The

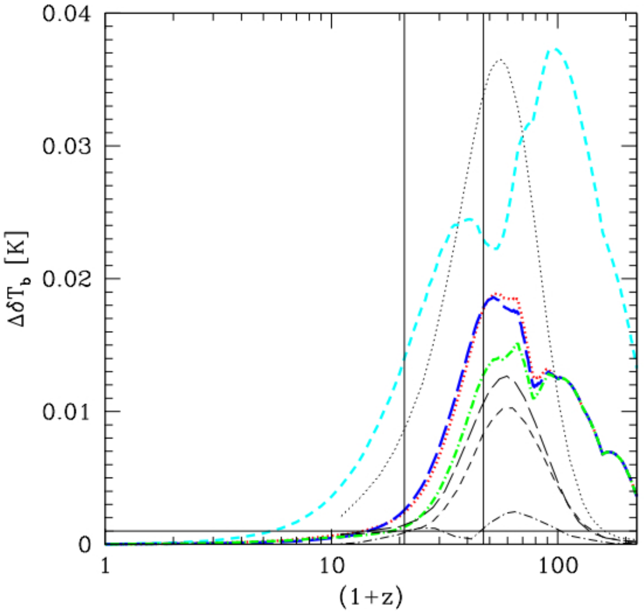

Figure 11. The difference of 21cm differential brightness temperature ($\Delta\delta T_b(z)$) for different cases, assuming a maximal absorption fraction and the clumpiness of the DM. Our results are shown as thick lines. The different line-styles are assigned in the same way as in Figure 7. For comparison, we also include the results obtained by Cumberbatch, Lattanzi & Silk (2010) for the case of SUSY models with a NFW density profile, taken from the upper panel of Figure 10 of the authors, and we show them as thin lines. The line-styles for the thin curves correspond to dot-dashed for Model 4, short-dashed for Model 2, long-dashed for Model 3 and dotted for Model1. We refer the reader to Table I of the authors for a description of the different models. We also include the detectability limits here discussed, corresponding to the 1 mK threshold and to the $z = 20$ (Population III stars) and $z = 46$ (minimum frequency of 30 MHz) limits.

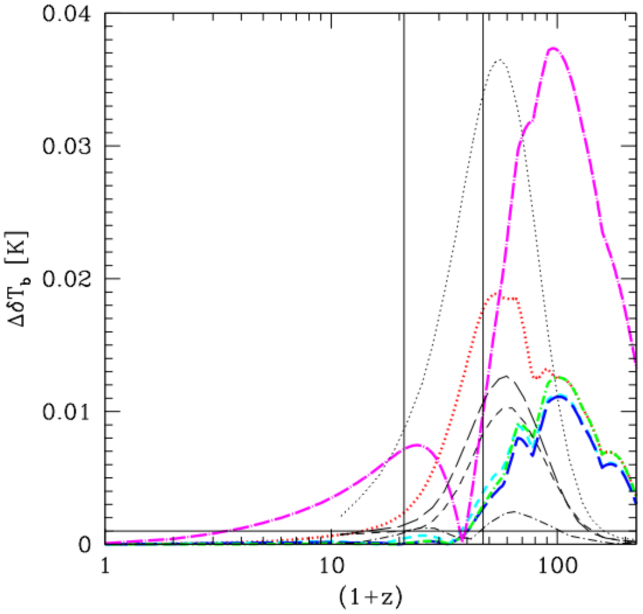

Figure 12. The difference of 21cm differential brightness temperature ($\Delta\delta T_b(z)$) for different cases, assuming a WIMP mass of 1TeV and substructure and clustering, or no DM clumpiness at all. Our results are shown as thick lines. The different line-styles are assigned in the same way as in Figure 8. For comparison, we also include the results obtained by Cumberbatch, Lattanzi & Silk (2010) for the case of SUSY models with a NFW density profile, taken from the upper panel of Figure 10 of the authors, and we show them as thin lines. The line-styles for the thin curves correspond to dot-dashed for Model 4, short-dashed for Model 2, long-dashed for Model 3 and dotted for Model1. We refer the reader to Table I of the authors for a description of the different models. We also include the detectability limits here discussed, corresponding to the 1 mK threshold and to the $z = 20$ (Population III stars) and $z = 46$ (minimum frequency of 30 MHz) limits.

$10GeV$ case is well within this window, due to its broad, secondary peak around $z \sim 30$, caused by the DM clustering. This same feature can be seen in the $\Delta\delta T_b$ curve of the $1TeV$ case with adiabatic compression and substructure, although the intensity of the signal is considerably lower, and the peak is now the primary peak. In the case of the $\Delta\delta T_b$ signal, the presence of substructure is more important than the presence of adiabatic compression. At least in principle, this signal could be detected for all the cases with $f_{abs} = 1$ that consider clumpiness.

It can be seen in Figure 12, that even in the no-clumpiness case, a WIMP with mass of $10GeV$ would still be inside the sensitivity window mentioned before, due to the broad peak in the signal around $z \sim 100$ and the secondary peak around $z \sim 25$. Also, for the cases with $1TeV$ WIMP but non-maximal f_{abs} or no clumpiness, the signal would be much weaker (on the $\sim 1-3mK$ level) and would just barely fall in the sensitivity window (at $40 < z < 46$), because the diminishing of the absorption fraction or the clumpiness would tend to shift the signal to redshift ~ 100.

It is important to keep in mind that, as was mentioned above, the sensitivity window here considered is only nominal, because the foreground extraction and the decontamination of the signal may be difficult.

We also present in Figure 11 and Figure 12 the $\Delta\delta T_b(z)$ curves obtained by Cumberbatch, Lattanzi & Silk (2010) and compare them with the results that we obtain.

It can be seen from the comparison between the curves given by the authors and ours, that the dynamical range of the values for the obtained $\Delta\delta T_b(z)$ curves are similar, but that the particular shapes of the curves are different. This may be because the authors use an analytic approximation to $\sigma(M, Z)$, and assume a pure power-law shape for the substructure, without considering time evolution of substructures within particular haloes, and so their curves will be more soft, having less numerical noise from the integration and equation solving procedures. For the case of maximal absorption fraction, and standard clustering, with a WIMP mass of $1TeV$, we find that the signal is peaked around redshift 50, in agreement with the results obtained by the authors, but for the cases with non-maximal absorption and less or no clustering, our curves are more displaced towards z∼100. It is interesting to note, however, that the curves presented by the authors already consider the absorption fraction explicitly.

7 CONCLUSIONS

In this paper, we develop formalisms for calculating the generated and received DM self annihilation luminosity of individual halos, as well as the energy injection rate per baryon in the universe as a whole, accounting for the clustering of the DM at all scales but without considering Sommerfeld enhancement. We also compute the effects on the IGM and on the 21cm signal of this extra energy injection due to the DM.

It is important to mention that we take a numeric approach for performing the calculations of the barionic clumpiness, instead of the analytic approach used by previous authors. Also, we incorporate adiabatic compression, which had not been done so far. The prescriptions used for the computations are the primordial power spectrum, the transfer function, the window function, the substructure mass function and its corresponding time evolution, the computation of the NFW parameters as a function of halo mass and redshift and the computation of the adiabatically compressed density profile for each halo.

We now give some general conclusions about the results obtained.

As discussed in Section 4.2, the luminosity generated within individual halos, considering $1TeV$ WIMPs, is not enough to self-regulate the star formation of the halo, and thus, it cannot contribute significantly to the standard feedback mechanisms (AGN feedback for galaxy cluster-sized haloes of mass greater than $10^{14} M_{\odot}$). In the case of a $10GeV$ WIMP and considering clustering by substructure and adiabatic compression, for haloes of masses greater than $10^{15} M_{\odot}$, DM annihilation may indeed contribute significantly (even more than AGN feedback) to the total energy injection into the Intra-Cluster Medium (ICM). The latter case however, considers a WIMP mass that is not the most favoured one. Also, virialized DM haloes of masses greater than $10^{15} M_{\odot}$ are rare even at redshift zero. At higher redshifts, high mass haloes are increasingly rare, and therefore, the importance of DM annihilation as a feedback mechanism is further diminished.

DM clustering in general is determinant in order to assess the effects of DM annihilation on the IGM and for computing the energy injection per baryon. Evidence of this are the clumpiness factors obtained in Section 4.4, which can be in excess of 10^6 at redshift zero (the energy injection rate is thus boosted by this factor with respect to the case of a perfectly smooth universe). Also, in favour of the importance of clustering are the results obtained for the ionization fraction $x_e(z)$ and the IGM kinetic temperature $Tk_{IGM}(z)$ discussed in Section 6.1 and Section 6.2, where it is clearly seen that, for the cases assuming a perfectly homogeneous universe, and for a WIMP mass of $1TeV$, the obtained evolutions of these quantities are virtually indistinguishable from the standard case with no energy injection due to DM. For example, not accounting for substructure, led Mapelli, Ferrara & Pierpaoli (2006) to conclude that the effects of a heavy ($\sim 100GeV$) neutralino on the IGM were negligible, and it was shown by Cumberbatch, Lattanzi & Silk (2010) that this may not be the case by accounting for the clustering of DM.

We find that the presence of annihilating and clumped DM may result in significant deviations in the evolutions of the inferred temperature and ionization fraction. For example, in the scenario that takes into account the clustering of DM at all levels, as well as the adiabatic compression, a $1TeV$ WIMP with thermal relic annihilation cross-section may, for example maintain the temperature of the IGM on the $\sim 100K$ level, or contribute to the ionization fraction maintaining it at a value of $\sim 10^{-2}$, until redshift zero (not considering POPIII stars). We conclude that although the DM annihilation can have a significant impact on the inferred properties of the IGM, it cannot be regarded as an alternative reionization scenario, because even in the case of a $10GeV$ WIMP (with lower mass than favoured by indirect detections and accelerator constraints), the value of x_e at $z < 100$ does not rise over 0.1. This is in agreement with the results obtained by Mapelli, Ferrara & Pierpaoli (2006), where for all the different models of decaying or annihilating DM considered by the authors, they obtained values of x_e at $z < 100$ of at most 0.3 (for the case of axino-type Light Dark Matter with a mass of $10MeV$ and without considering POPIII stars). We note however that among the models that they considered, only the neutralino DM model is comparable to our results for the no clumpiness case. Both results are in good agreement, however we do not use exactly the same mass as they do, and we do not consider cross-section enhancement. Varying the mass of the WIMP and considering a constant enhancement in cross-section can have enormous effects on the properties of the IGM as the DM energy injection rate scales as $\propto \frac{<\sigma v>}{m_\chi}$ (disregarding the variation in the presence of substructure when changing m_χ due to free-streaming effects).

About the detectability of the $21cm$ $\Delta\delta T_b$ signal, defined as the absolute value of the difference of the differential brightness temperatures in 21cm with and without DM energy injection (see Section 6.5), we can conclude considering the results that we obtain that, according to the sensitivity limits mentioned by Valdés et al. (2007), and considering a maximal absorption fraction $f_{abs} = 1$, a thermal relic WIMP with mass of $1TeV$ may have a signal detectable at the $\sim 15mK$ level, peaked around $z \sim 50$ (corresponding to a frequency of $\sim 30MHz$; see Section 6.5). For lower absorption fractions, a $1TeV$ WIMP may not be detectable by the $21cm$ signal. A lower mass WIMP may be detectable, although a mass on the order of $\sim 10GeV$ or lower is not favoured by neither accelerator constraints (see Section 2.3), nor indirect detection searches (see Section 4.6). Comparing with the results obtained by Cumberbatch, Lattanzi & Silk (2010), we notice that for their different SUSY neutralino models, the authors obtain $\Delta\delta T_b$ curves that cover a similar dynamic range than our curves. However, in the redshift range of $20 < z < 46$ that is interesting for detection, they tend to predict a stronger signal than our $1TeV$ WIMP with $f_{abs} = 0.01$ case, to which we should compare their results to (because the authors already incorporate an explicit f_{abs} treatment and they have values $f_{abs} \sim 0.01$ in that redshift range; see their figure 12 and figure 13). This may be simply because they use a lower mass $50GeV$ WIMP, but they obtain the energy and number of photons and electron-positron pairs that result from the cascades produced by the primary products of the annihilation and use these in order to compute f_{abs}. Their results in the interesting redshift range are however similar to our $f_{abs} = 1$ maximal absorption case with a $1TeV$ WIMP. According to their results, all of their SUSY models would be in principle detectable, except for their model 4 (see their Table 1 for more details).

Finally, as future work, we should mention that it is in principle possible to use the DM annihilation luminosity received by a halo (Section 5), together with the luminosity generated by the halo itself (Section 4.2), in order to compute the effects that the extra energy injection will have on the standard physical processes that take place in the barionic component of the halo (Intra Cluster Medium or ICM in the case of galaxy cluster-sized haloes), like for example its neutral hydrogen abundance, Bremsstrahlung luminosity, etc... Also, being able to compute the ionization fractions and temperatures of individual haloes at high redshifts, as well as their spatial clustering, may provide a way of computing the angular fluctuations of the differential brightness temperature (δT_b) signal for different WIMP scenarios, in order to have another test besides the predicted global signal. These issues will be explored in a future paper.

8 ACKNOWLEDGEMENTS

IJA is currently supported by CONICYT (Comisión Nacional de Investigación Científica y Tecnológica - Chilean Government) and by the Fulbright commission through a joint fellowship. IJA is also supported by the Physics and Astronomy Department of the University of Southern California. Part of this work was conducted while IJA was studying at Pontificia Universidad Católica de Chile and he was supported in part by BASAL-CATA (Centro de Astronomía y Tecnologías Afines - Chile) PFB-06, and Fondecyt #1110328. Part of the calculations performed for this work were carried out using the Geryon cluster at the Centro de Astro-Ingeniería of Pontificia Universidad Católica de Chile.

References

Abdo, A. A., et al. 2009, Phys. Rev. Lett. 102, 181101

Adriani, O., et al. 2009, Nature 458, 607

Aharonian, F., et al. 2008, Phys. Rev. Lett. 101, 261104

Angulo, R. E., White, S. D. M. 2010, MNRAS 401, 1796

Appelquist, T., Cheng, H. C., Dobrescu, B. A. 2001, Phys. Rev. D 64, 035002

Arkani-Hamed, N., Finkbeiner, D. P., Slatyer, T. R., Weiner, N. 2009, Phys. Rev. D 79, 015014

Bardeen, J. M., Bond, J. R., Kaiser, N., Szalay, A. S. 1986, ApJ 304, 15

Binney, J., Tremaine, S. 1987, Galactic Dynamics (Princeton Univ. Press)

Blumenthal, G. R., Faber, S. M., Flores, R., Primack, J. R. 1986, ApJ 301, 27

Blumenthal, G. R., Faber, S. M., Primack, J. R., Rees, M. J. 1984, Nature 311, 517

Bond, J. R., Efstathiou, G. 1984, ApJ 285, L45

Bond, J. R., Cole, S., Efstathiou, G., Kaiser, N. 1991, ApJ 379, 440

Cline, J. M., Vincent, A. C., Xue, W. 2010, arXiv, arXiv:1001.5399v2

Cumberbatch, D. T., Lattanzi, M., Silk, J. 2010, arXiv, arXiv:0808.0881v3

D'Amico, G., Kamionkowski, M., Sigurdson, K. 2009, arXiv, arXiv:0907.1912v1

Diemand, J., Kuhlen, M., Madau, P., Zemp, M., Moore, B., Potter, D., Stadel, S. 2008, Nature 454, 735

Dolag, K., Vazza, F., Brunetti, G., Tormen, G. 2005, MNRAS 364, 753

Dunkley, J. et al. [WMAP collaboration] 2009, ApJS 180, 306

Elsässer, D., Mannheim, K. 2004, Astropart. Phys. 22, 65

Finkbeiner, D. P., Goodenough, L., Slatyer, T. R., Vogelsberger, M., Weiner, N. 2010, arXiv, arXiv:1011.3082v1

Gao, L., White, S. D. M., Jenkins, A., Stoehr, F., Springel, V. 2004, MNRAS 355, 819

Giocoli, C., Pieri, L., Tormen, G. 2008, MNRAS 387, 689

Giocoli, C., Pieri, L., Tormen, G., Moreno, J. 2009, MNRAS 395, 1620

Giocoli, C., Tormen, G., van den Bosch, F. C. 2008, MNRAS 386, 2135

Hamilton, A. J. 2001, MNRAS 322, 419

Hannestad, S., Tram, T. 2010, arXiv, arXiv:1008.1511v1

Hinshaw, G. 2009, ApJS 180, 225

Hirata, C. M. 2006, MNRAS 367, 259

Hooper, D., Goodenough, L. 2010, arXiv, arXiv:1010.2752v1

Hooper, D., Profumo, S. 2007, Physics Reports 453, 29

Hooper, D., Finkbeiner, D. P., Dobler, G. 2007, Phys. Rev. D 76, 083012

Jungman, G., Kamionkowski, M., Griest, K. 1996, Physics Reports 267, 195

Kaluza, T. 1921, Sitzungsber. Preuss. Akad. Wiss. Berlin (Math. Phys.) 1921, 966

Kamionkowsky, M., Koushiappas, S. M., Kuhlen, M. 2010, arXiv, arXiv:1001.3144v2

Kauffmann, G., Colberg, J. M., Diaferio, A., White, S. D. M. 1999, MNRAS 303, 188

Kolb, E. W., Turner, M. S. 1990, The Early Universe (Westview Press)

Komatsu, E., et al. [WMAP collaboration] 2011, ApJS 192, 18
Kuhlen, M., Madau, P., Montgomery, R. 2006, ApJ 637, L1
Lacey, C., Cole, S. 1993, MNRAS 262, 627
Lagos, S. del P., Cora, S. A., Padilla, N. D. 2008, MNRAS 388, 587
Laor, A. 1996, arXiv, arXiv:astro-ph/9609163v1
Liszt, H. 2001, A&A 371, 698
Longair, M. S. 1998, Galaxy Formation (Springel-Verlag)
Mapelli, M., Ferrara, A., Pierpaoli, E. 2006, MNRAS 369, 1719
Martin, S. P. 2008, arXiv, arXiv:hep-ph/9709356v5
Mo, H. J., White, S. D. M. 1996, MNRAS, 282, 347
Murray, N., Quataert, E., Thompson, T. A. 2005, ApJ 618, 569
Natarajan, A., Schwarz, D. J. 2009, Phys. Rev. D 80, 043529
Natarajan, P., Croton, D., Bertone, G. 2008, MNRAS 388, 1652
Navarro, J. F., Frenk, C. S., White, S. D. M. 1997, ApJ 490, 493
Paczyński, B. 1987, Nature 325, 572
Pengelly, R. M. 1964, MNRAS 127, 145
Pieri, L., Bertone, G., Branchini, E. 2008, MNRAS 384, 1627
Pierpaoli, E. 2004, Phys. Rev. Lett. 92, 3
Piffl, T., Sotnikova, N. Ya. 2008, arXiv, arXiv:0811.2573v1
Pinzke, A., Pfrommer, C., Bergstrom, L. 2009, arXiv, arXiv:0905.1948v3
Press, W. H., Schechter, P. 1974, ApJ 187, 425
Quinlan, G. D., Hernquist, L., Sigurdsson, S. 1995, ApJ 440, 554
Raffelt, G. G. 1997, arXiv, arXiv:hep-ph/9712538v1
Raffelt, G. G. 2008, Lect. Notes Phys. 741, 51
Ripamonti, E., Mapelli, M., Ferrara, A. 2007, MNRAS 374, 1067
Rubin, V. C., Ford, W. K. 1970, ApJ 159, 379
Ryden, B. 2003, Introduction To Cosmology (Addison Wesley)
Sellwood, J. A., McGaugh, S. S. 2005, ApJ 634, 70
Sheth, R. K., Mo, H. J., Tormen, G. 2001, MNRAS 323, 1
Spergel, D. N., et al. [WMAP collaboration] 2003, ApJS 148, 175
Springel, V., et al. 2005, Nature 435, 629
Springel, V., et al. 2008, MNRAS 391, 1685
Sreekumar, P., et al. 1998, ApJ 494, 523
Taylor, J. E., Babul, A. 2004, MNRAS 348, 811
Valdés, M., Ferrara, A., Mapelli, M., Ripamonti, E. 2007, MNRAS 377, 245
Yamamoto, K., Sugiyama, N., Sato, H. 1998, ApJ, 501, 442
Young, P. ApJ 242, 1232
Zehavi, I., et al. 2011, ApJ 736, 59
Zwicky, F. 1933, Helv. Phys. Acta 6, 110